TECHNICAL REPORT NO. 3-545

STRESSES UNDER MOVING VEHICLES

Report 5

DISTRIBUTION OF STRESSES BENEATH A TOWED PNEUMATIC TIRE IN AIR-DRY SAND

by

A. J. Green, Jr.
N. R. Murphy, Jr.

July 1965

Sponsored by

U. S. Army Materiel Command
Project No. 1-V-0-21701-A-046
Task 03

Conducted by

U. S. Army Engineer Waterways Experiment Station
CORPS OF ENGINEERS
Vicksburg, Mississippi

ARMY-MRC VICKSBURG, MISS.

FOREWORD

This report is the fifth in a series presenting results of studies conducted to determine the magnitude and distribution of stresses under moving vehicles. The study reported herein was conducted at the U. S. Army Engineer Waterways Experiment Station under the sponsorship and guidance of the Directorate of Research and Development, U. S. Army Materiel Command, as part of DA Project 1-V-0-21701-A-046, "Trafficability and Mobility Research," Task 1-V-0-21701-A-046-03, "Mobility Fundamentals and Model Studies."

The tests were conducted by personnel of the Army Mobility Research Branch (AMRB), Mobility and Environmental Division, under the supervision of Messrs. W. J. Turnbull, Technical Assistant for Soils and Environmental Engineering; W. G. Shockley, Chief, Mobility and Environmental Division; S. J. Knight, Chief, AMRB; and D. R. Freitag, Chief, Mobility Section. Mr. A. J. Green, Jr., had the primary responsibility for conduct of the tests and the preparation of this report. Mr. H. B. Boyd participated in the conduct of the tests. Mr. N. R. Murphy, Jr., assisted in the preparation of this report.

Directors of the Waterways Experiment Station during the course of the investigation and the preparation of this report were Col. Edmund H. Lang, CE, Col. Alex G. Sutton, Jr., CE, and Col. John R. Oswalt, Jr., CE. Technical Director was Mr. J. B. Tiffany.

CONTENTS

SUMMARY

This report presents the results of a study conducted to determine the magnitude and distribution of stresses normal to the tire-soil interface of an 11.00-20, 12-PR, smooth pneumatic tire towed in an air-dry sand. Data such as the induced stresses in the soil mass and the deflected shape of the moving tire were also obtained.

Seven pressure cells in the tire carcass measured the magnitude of stresses at the tire-soil interface. The results indicated that the stress distribution patterns are strongly related to the shape of the moving tire and that the shape (deflection) of the tire was influenced by load, inflation pressure, and soil strength. Peak stresses induced in the soil mass by the moving tire occurred well ahead of the axle. The total load on the wheel had the greatest influence on the magnitude of the stresses deep within the soil mass.

The average stress waves for a tire-soil system such as used in this study can be expressed mathematically in terms of a Fourier series. Application of the Fourier series in stress wave analysis is discussed in Appendix A.

STRESSES UNDER MOVING VEHICLES

DISTRIBUTION OF STRESSES BENEATH A TOWED PNEUMATIC TIRE IN AIR-DRY SAND

PART I: INTRODUCTION

Background

1. One of the research programs being conducted under the Trafficability and Mobility Research projects is directed toward the attainment of a better understanding of the interaction of vehicle running gear and soft soils. This understanding should lead to the improvement of military vehicles from the standpoint of their ability to travel across natural terrain.

2. Knowledge of the magnitude and distribution of stresses and strains in soil yielding under a loaded pneumatic tire would be a major advance in the study of tire-soil relations. Studies have been conducted at the Waterways Experiment Station (WES) on the deflection of pneumatic tires on yielding and unyielding surfaces.[1*] Direct measurement of the stresses imparted by the moving tire to the soil mass on which it travels has also been attempted using pressure cells embedded in the soil, but precise measurement of stresses proved difficult.[2] Pressure cells installed in soft soil move with the soil as it yields under traffic, and it is virtually impossible to determine the exact orientation of the cells when pressures are being registered.

3. It was considered that cells installed in the carcass of the tire would provide more accurate stress measurements at the tire-soil interface, since the orientation of these cells can be determined by means of deflection gage measurements of the shape of the deflected cross section and circumference of the test tire.

4. A pilot study of stress distribution beneath pneumatic tires was conducted with cells placed in a smooth, nonyielding surface. These measurements are reported in reference 2d.

---

* Raised numerals refer to similarly numbered items in the Literature Cited at end of text.

Purpose and Scope

5. The primary purpose of the investigation reported herein was to determine the magnitude and distribution of stresses normal to the surface of a towed pneumatic tire operating in an air-dry cohesionless soil. Of secondary importance during the investigation were the measurement of the stresses within the soil mass, the determination of the shape of the moving tire, and the collection of data on towed force, sinkage, and slip of the tire.

6. The investigation was limited to tests with an 11.00-20, 12-PR, smooth pneumatic tire towed in an air-dry, coarse-grained soil. Most of the tests were conducted on soil at three strengths that can be categorized by the cone index ranges 15 to 17, 25 to 28, and 55 to 60. Inflation pressures of 15, 30, and 60 psi were employed at wheel loads of 1500, 3000, and 4500 lb for each soil condition.

Definitions

7. Certain special terms used in this report are defined below, and some of them are illustrated graphically in fig. 1.

Cell mount. The housing for a pressure cell or group of pressure cells.

Contact area. The portion of the tire in contact with the supporting surface. Interruptions of the contact area due to tread patterns are considered part of the contact area. (Synonyms are contact patch and tire-soil interface.)

Contact length. Maximum length of the contact area, measured parallel to the plane of rotation of the tire.

Contact width. Maximum width of the contact area, measured perpendicular to the contact length.

Tire deflection. Any displacement of a point on the tire surface from its position on the inflated but unloaded tire.

Deflection (percent). $\frac{\text{Tire deflection}}{\text{Carcass section height}} \times 100$.

Maximum hard-surface deflection (δ_{MH}). Difference between carcass section height and loaded carcass section height (see fig. 1).

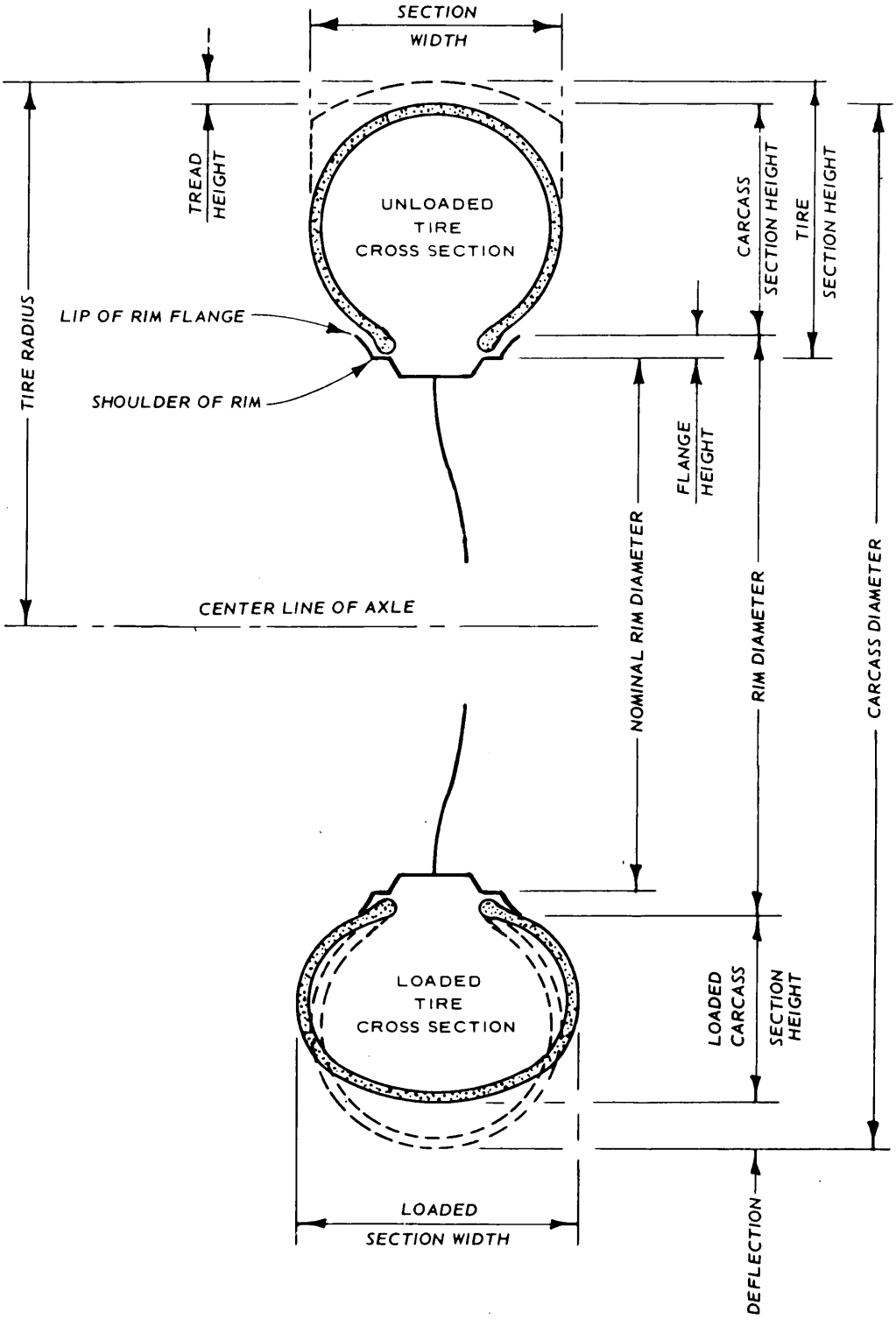

NOTE: PERCENT DEFLECTION = $\frac{\text{DEFLECTION}}{\text{CARCASS SECTION HEIGHT}} \times 100.$

Fig. 1. Dimensional terminology for tire and rim

Maximum in-soil deflection (δ_{MS}). Maximum deflection measured on the center line of the cross section of the tire as it moves in the soil. Its magnitude depends upon load, inflation pressure, and soil strength.

Towed force (P_T). Pull at the towed condition.

Sinkage (z). Maximum depth to which the wheel penetrates the soil relative to the original soil surface.

Rut depth. Depth of rut, relative to the original soil surface, after passage of the wheel. (May differ from sinkage because of soil rebound or fill-in.)

Travel ratio. Ratio of the actual wheel advance per revolution to the theoretical advance per revolution.

Slip. Unity minus the travel ratio where the theoretical wheel advance per revolution is taken as the hard-surface rolling circumference. Slip is usually expressed as percentage.

Reference plane (vertical). A vertical plane through the center line of the axle of the test wheel.

Reference plane (horizontal). A horizontal plane tangent to the lowest point on the circumference of the deflected test tire.

PART II: TEST FACILITIES, EQUIPMENT, AND TECHNIQUES

Type of Soil Used

8. The soil used for these tests was an air-dry, poorly graded, medium-to-fine mortar sand, subangular in shape, and classified as SP in the Unified Soil Classification System. Gradation and classification data for the soil are shown in fig. 2. The average moisture content during the tests was 0.2 percent. The sand was placed in an open pit approximately 4-1/2 ft wide, 100 ft long, and 3-1/2 ft deep, that had been lined with waterproof membrane.

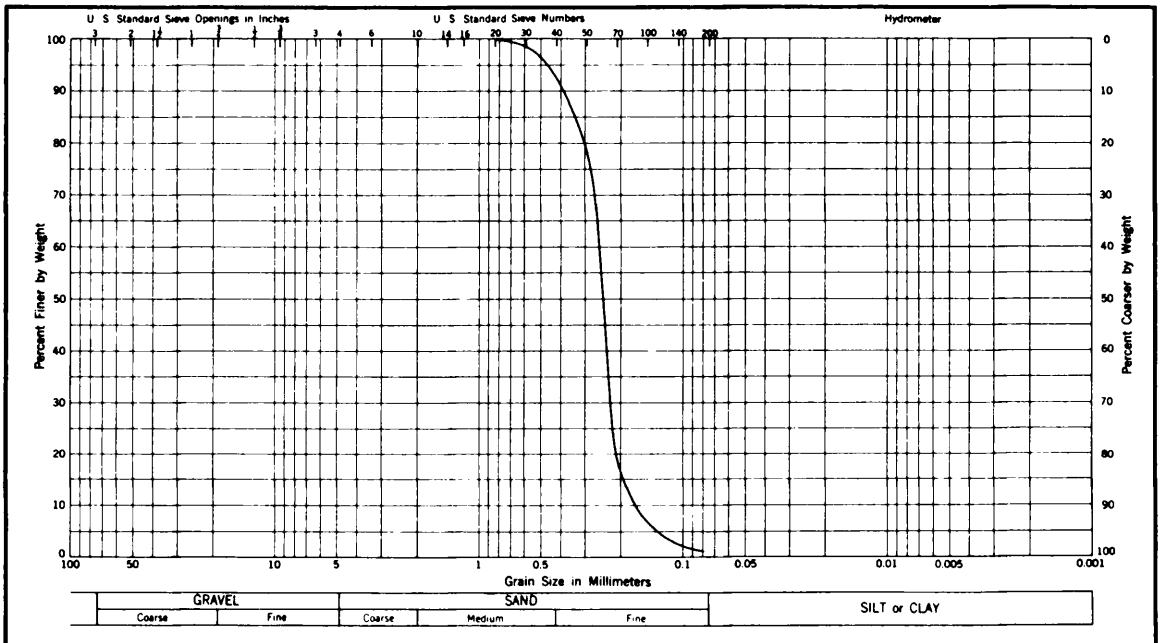

Number	Depth	Natural Moisture	L. L.	P. L.	P. I.	Classification		
							MAX DENSITY	MIN DENSITY
						SAND (SP)	106 1	87 4

MORTAR SAND

Fig. 2. Soil gradation and classification data

Soil Preparation Procedures

9. The sand was placed in the test pit in quantities sufficient to result in layers approximately 6 in. deep after being leveled. Leveling

of the respective layers was accomplished with a section of grader blade or a 2- by 8-in. timber attached to the test carriage. The placing and leveling were repeated until the pit was filled, after which processing and compaction were accomplished as follows. The sand was tilled with a multiple-tooth harrow (scarifier) that was pulled back and forth through the pit until adequate loosening of the sand was attained. Maximum tillage depth was 36 in. The sand was compacted by towing a vibrator on a steel sled back and forth over the surface until the desired soil strength profile had been produced. The depth of tillage and the amount of compaction necessary for each test varied, depending both upon the soil strength required and upon the existing strength after previous traffic on the pit. The tools used for tilling and compacting (scarifier and vibrator) were attached to the test carriage and towed at a uniform speed (about 1.0 fps). The goal of the soil processing was to obtain a strength profile such that the strength increased uniformly with depth and was consistent along the length of the test lane. Cone index measurements were made before each test to evaluate the effectiveness and uniformity of the processing. Average cone index-depth profiles for the high- and low-strength sands tested are shown in fig. 3.

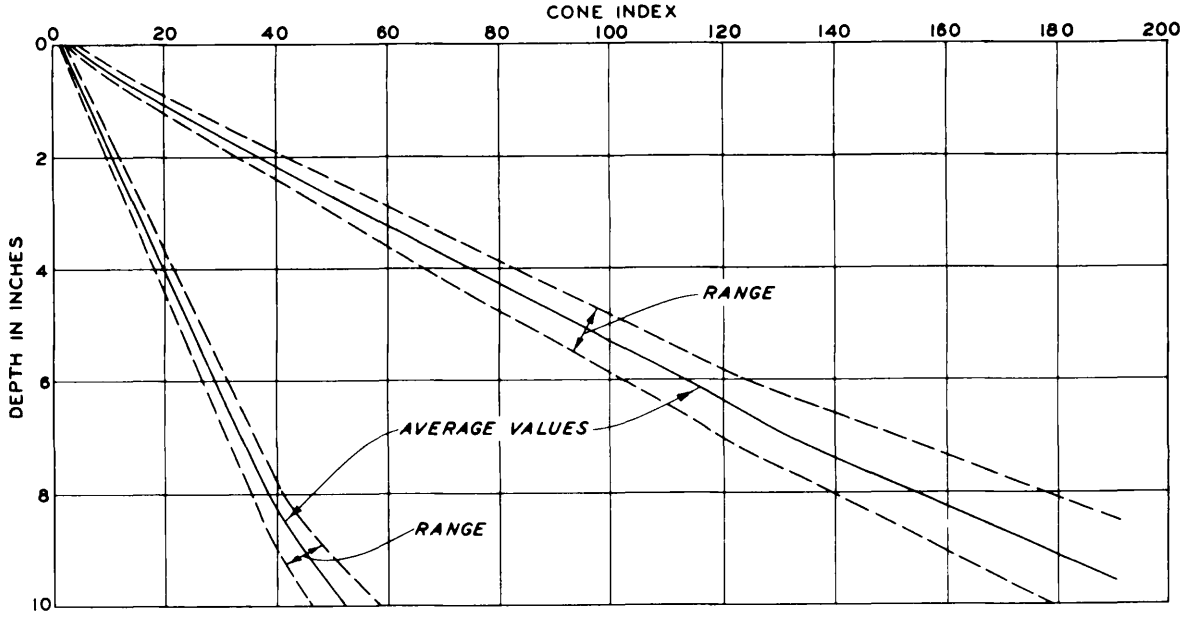

Fig. 3. Average cone index profiles, low- and high-strength sands

Pressure Cell Installation in Soil

10. Three commercially available pressure cells of the deflecting diaphragm type, 0.5 in. in diameter, were used to measure the stresses produced in the soil mass during the passage of the wheel. The maximum rated capacity of this type of cell is 25 psi, and the manufacturer states that the calibration of the cell is linear within ±0.6 percent throughout this range. The calibration factor for this type of cell is approximately 310 microinches per psi, or a total deflection of 7750 microinches when the applied pressure is 25 psi. Brass mounts 3 in. in diameter and 1 in. thick were used to house the cells.[3] The cells were buried beneath the center line of the intended tire path at various depths. Since results of earlier programs led to the conclusion that cells that are displaced with the soil during traffic gave results that were difficult, if not impossible, to evaluate, the cells were installed at depths where stresses were expected to be of measurable magnitude, but not high enough to cause significant cell movement. In the earlier tests, the cells were installed in the testing area after construction of the pit was completed. They were buried beneath the center line of the intended tire path at various depths ranging from 12 to 24 in. with the minimum horizontal spacing between the cells being 3 ft. After the cells had been placed, the soil above them was replaced and compacted manually. However, this practice was found to destroy the uniformity of the test section and was therefore discontinued. The next procedure used involved placing the cells in the desired position, loosely replacing the sand above them, then processing the entire test section, and conducting a tire test without further checking the cell position. When this procedure was first used, the cells were uncovered after each test (including one during which large tire sinkage occurred) and it was found that they had not moved. Therefore, in the latter part of the program the cell positions were checked only after every fifth test. During the entire period of using this procedure, the cells were buried beneath the center line of the intended tire path at a depth of 18 in., with a minimum horizontal spacing of 3 ft.

Single-Wheel Test Dynamometer

Test carriage

11. The test carriage used in these tests can accommodate wheels up to 56 in. in diameter and 26 in. in width. The carriage controls the path and alignment of the test wheel and is designed to isolate and measure the resultant horizontal and vertical forces and the torque at the wheel. Devices for determining degrees of tire rotation, forward travel of the test carriage, and vertical movement of the hub of the test wheel are part of the system. Fig. 4 shows an overall view of the test carriage. Details of the instrumentation necessary to measure the forces are presented in another report.[3]

Sinkage-measuring device

12. The sinkage-measuring device consisted of a circular potentiometer with a threaded pulley affixed to its shaft. Several turns of steel wire were wound onto the pulley to prevent slippage; one end of the wire was attached to a small weight to produce tension in the wire, while the other end was attached to the innermost frame (containing the wheel) of the test carriage, near its center point. The rotation of the potentiometer was calibrated to record the linear movements. This sinkage-measuring device was used to determine the vertical displacement of the axle of the wheel during the test.

Event markers

13. A photoelectric event marker was used to determine the carriage position and speed. For each foot that the center of the test wheel axle traveled, the event marker produced a mark on the oscillogram. Since the oscillogram was automatically marked at intervals of 0.1 sec, the position and speed of the carriage (and the test wheel axle) could be determined for any instant. Another photoelectric event marker was used to determine the angular position of the test tire. For each 15 degrees of tire rotation, the event marker produced a mark on the oscillogram. The two event markers also made it possible to refer the location of all stress and deflection measurements to a common datum.

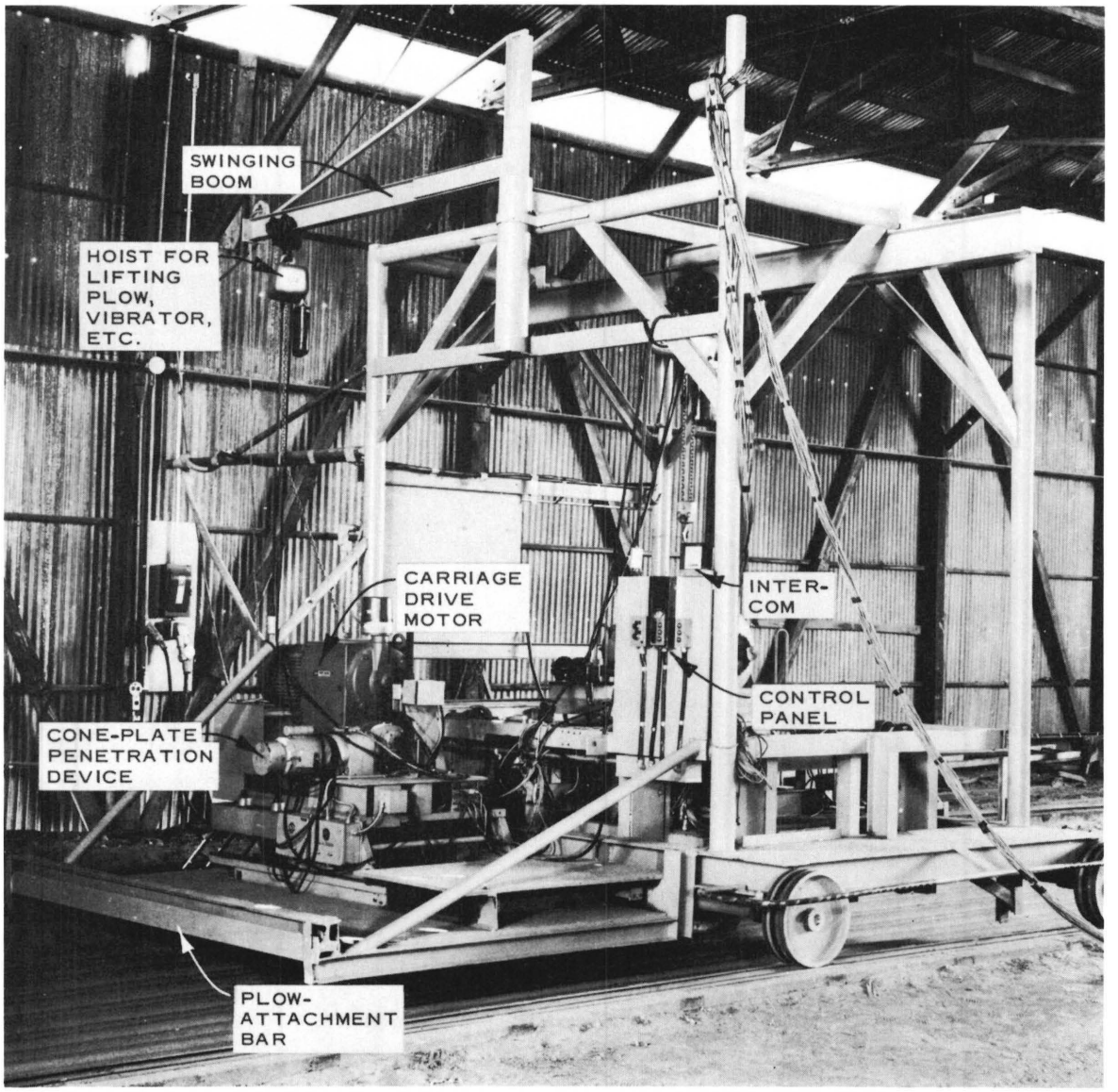

Fig. 4. Rear view of test carriage

Test tire

14. The tire used was an 11.00-20, 12-PR, NDCC military tire from which all tread had been removed by buffing. In buffing the tire, only the thickness of the lugs was removed so that the tire's carcass thickness and shape were very near the original thickness and shape. Deflection gages were mounted inside the tire to determine transient changes in shape of the cross section in the contact area during operation. Stress cells were placed in the tire so that their diaphragms were flush with the tire's outer surface, in order to measure normal stresses at

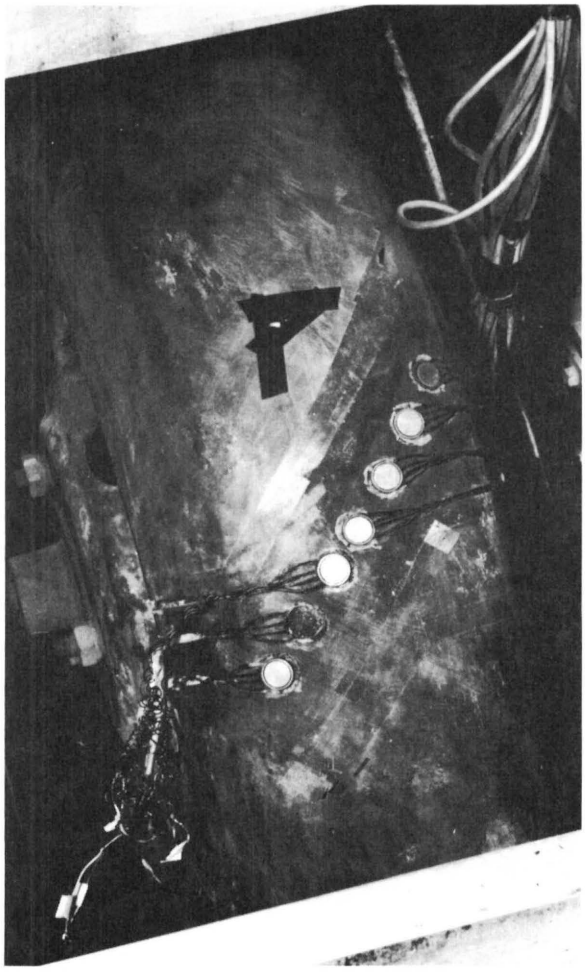

Fig. 5. Cells in the tire carcass

the tire-soil interface (fig. 5).

Stress cells

15. Seven, specially constructed, deflecting diaphragm cells, 0.75 in. in diameter and 0.25 in. high, were mounted in the face of the tire. A protective steel cup around each cell prevented the tire from exerting pressure on the cell's side walls, a necessary precaution since it was found that such a pressure caused the diaphragm to deflect and indicate a stress. The cup walls and bottom were 1/16 in. thick, and its inside radius was 1/32 in. larger than that of the cell. A semiconductor strain gage constituted the pressure-sensitive element of each cell, and resistors were used to complete a full Wheatstone bridge circuit. Since the semiconductor gage was 50 to 75 times more sensitive than an ordinary strain gage, the deflection of the cell's diaphragm could be relatively small. The maximum rated capacity of these cells is 50 psi. The calibration indicated that the cells were linear within $\pm$1.0 percent throughout the pressure range. The calibration factor for these cells is approximately 11.0 microinches per psi, or a total deflection of approximately 550 microinches when applied pressure is 50 psi. Fig. 6 is a schematic drawing of the cell and the electrical circuit from the cell to the recorder. Because the temperature changes during a specific test were relatively small, it was not necessary to design the cell for temperature compensation. Duplicate wires were connected to each end of the strain gage rather than the usual single wire, and in addition these wires were coiled so that they would bend without breaking as the tire flexed. This procedure greatly reduced the likelihood of a cell being rendered

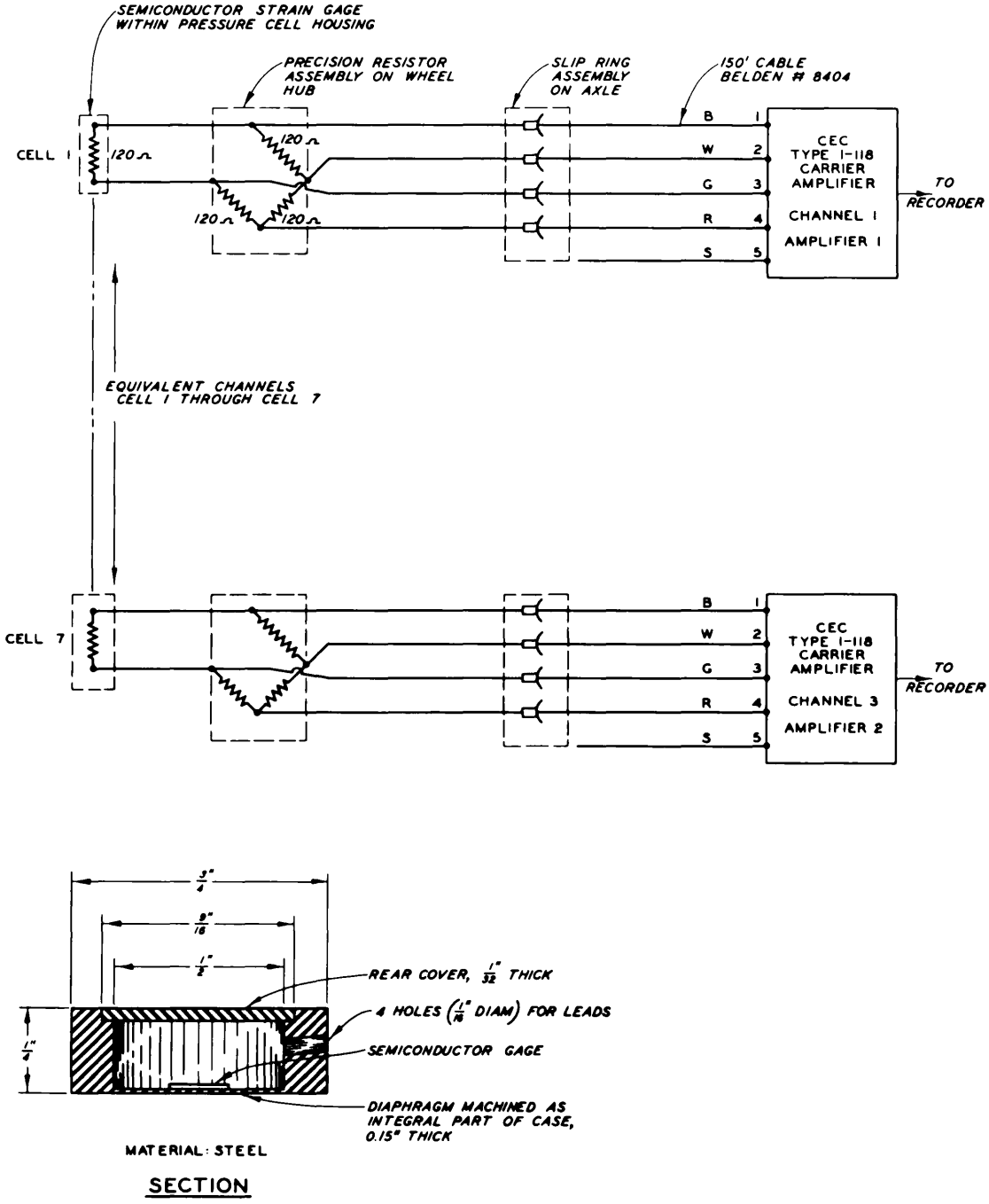

Fig. 6. Electrical schematic drawing of WES stress cell and amplifier

inoperative during a test because of wire damage.

16. Seven holes, each large enough to accommodate the cell and cup described in paragraph 15, were cut in the tire's outer surface; then slits were cut to contain the lead wires of each cell. The seven cells were installed along a diagonal line across the face of the tire (see fig. 5) to

avoid serious weakening of the tire in a single cross-sectional plane. The total depth of the cell and cup was approximately equal to the thickness of the rubber over the outermost layer of cord, and for this reason extreme care had to be taken when cutting the tire to avoid damage to the cords. The bottom of the cup was bonded to the tire with a latex-base adhesive. The area between the outer walls of the cup and the tire was backfilled with a pliable rubber-base compound. The cell was fastened to the cup with a thin layer of bituminous-base adhesive so that the cell would stay in place during traffic but could be removed easily for calibration or repair. A strip of thin rubber membrane was used to cover the entire cell area to prevent damage of the cell's diaphragm and to prevent sand from getting in the area between the cup and the wall of the cell. The membrane was fastened to the tire with a thin plastic adhesive tape that would deflect with the tire without providing additional stiffness to the tire carcass.

Deflection gages

17. Three types of deflection gages were utilized in this study (fig. 7). Types 1 and 2 measured only linear movement, whereas type 3 was

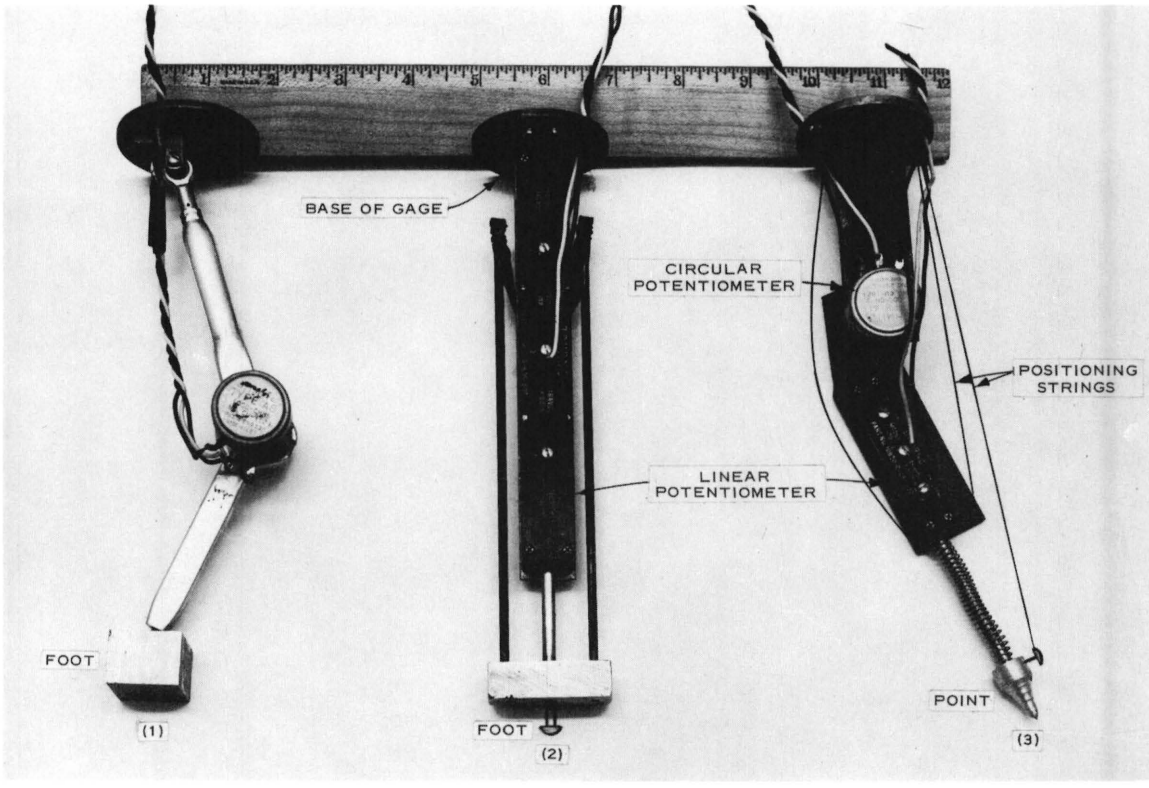

Fig. 7. Deflection gages

capable of measuring both translational and rotational movement of a point on the tire's inner surface. (Type 3 gages are referred to as linear-angular gages.) The linear and circular potentiometers used in these gages register a resistance change as the shaft of the potentiometer is moved. Five deflection gages were used during this study, and the location of each of the gages in the tire cross section is shown in fig. 8. The gages were

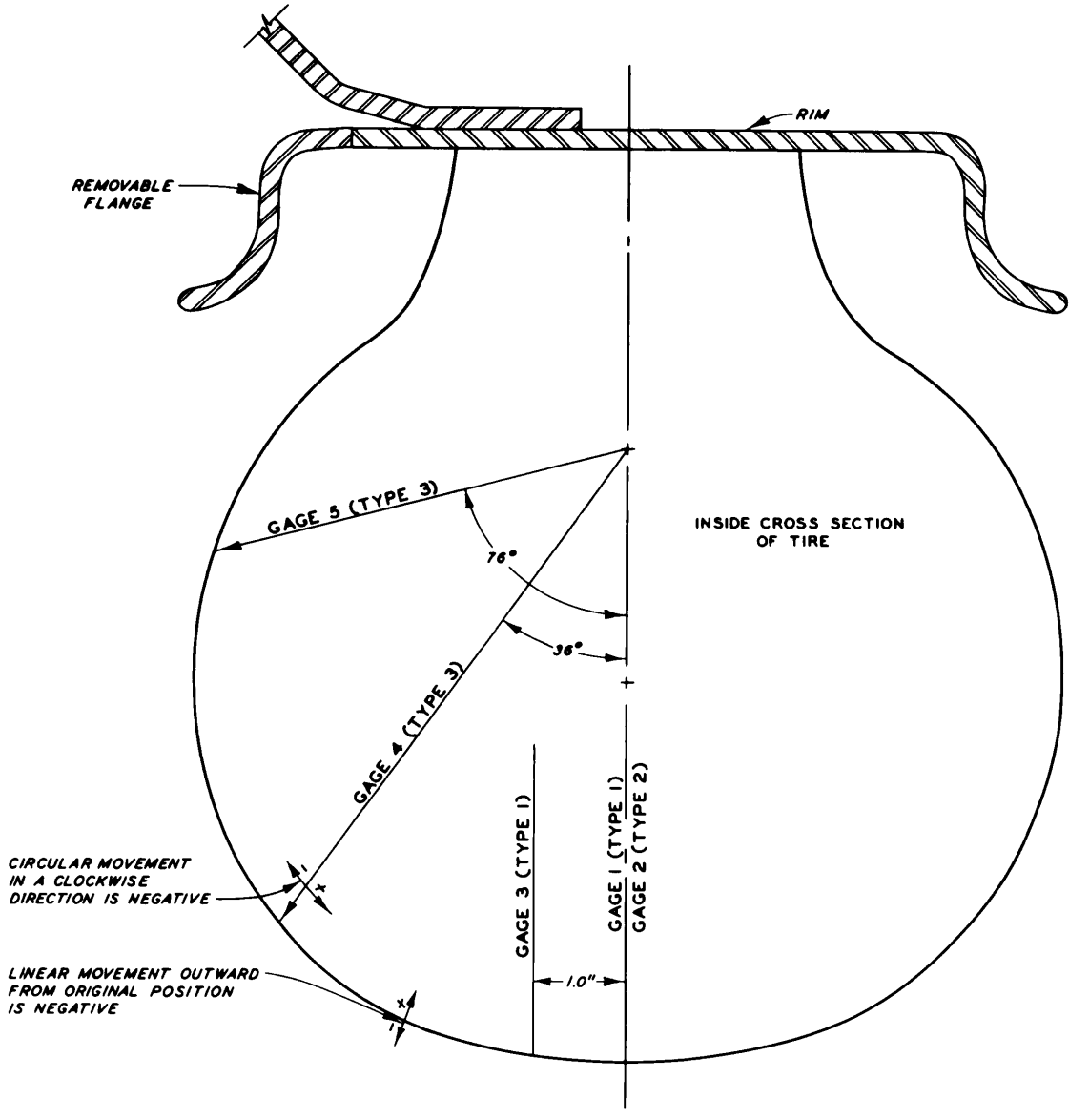

Fig. 8. Location of deflection gages in tire cross section

spaced at intervals of 30 degrees or more in the plane of tire rotation. Two gages were placed on the center line; three were placed on the left

(looking in the direction of travel) side of the cross section.

18. Mounting of the deflection gages in a tube-type tire required that the gage ports be sealed to the tube before being placed in the rim. Six holes were drilled in the rim, and six holes were cut in the tube to match those in the rim (fig. 9). The next step was to bond the deflection gage ports to the tube. The ports had an exterior flange that rested against the inner part of the tube. A threaded annular ring, with outside diameter the same as that of the flange, was tightened against the outside of

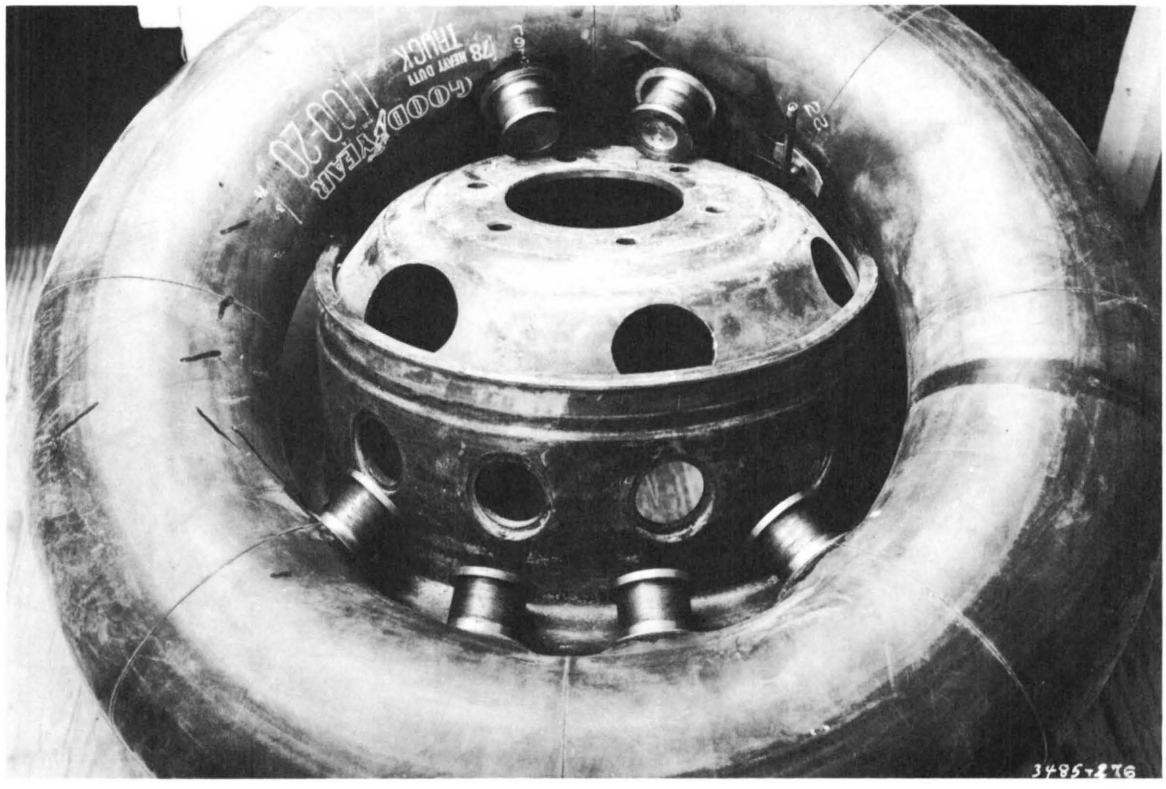

Fig. 9. Deflection gage ports in 11.00-20 tube

the tube and rubber-to-metal cement was used to help complete the seal. As the tire was mounted, the ports in the tube were pushed through the openings in the rim and then fastened to the rim with a locknut. The next step was the installation of the deflection gage. The ports in the tube had an inner flange upon which the base of the deflection gage (fig. 7, p 20) rested as a spacer. Since the position of the base of each gage relative to the center of the axle was often different, spacers or sleeves were placed between the base of the deflection gages and the inner flange of the ports.

A threaded annular ring was used to fasten the base of each gage port in position. Small holes in the base accommodated the electrical wires and the strings that were used to position the linear-angular gages. A cap was used to seal the top of the port, and hermetically sealed leads in this cap provided an outlet for the electrical wires from the deflection gages. During installation the foot of the "scissors" gage (see type 1, fig. 7) was cemented to the tube and then the installation continued in the manner described. The fixed gages (see type 2, fig. 7) required only that the base of the gage be oriented properly during installation, i.e. with the wider portion of the gage perpendicular to the direction of travel. The linear-angular gages were oriented so that they measured rotational movement in the plane of the cross section. The gage was rotated to the desired angular position while outside the tire, and the circuit that included the circular potentiometer was balanced at that position. The gage was then placed in the port, and the base was tightened in position. After this was done, the positioning strings were used to rotate the gage until the circular potentiometer circuit for that gage was rebalanced, indicating that the gage was in the desired position.

Test Procedures and Types of Data Obtained

Tire measurements

19. The load-inflation-deflection relations of the test tire on a nonyielding surface have been used to characterize the test conditions. At any constant load, different inflation pressures produce different amounts of deflection, different sizes of contact area, and different average contact pressures. Similarly, changes in load at constant inflation pressures produce differences in the parameters mentioned. The effects of different combinations of loads and inflation pressures for the test tire were determined and are listed in table 1.

Soil measurements

20. The strength of the soil in the test lane, in terms of cone index, was measured both prior to and during traffic. At intervals, measurements were made along the length of the test lane and averaged. The measurements made during traffic reflected the changes caused by the

applied loading. The loads, inflation pressures, and cone indexes pertaining to each of the tests reported herein are shown in table 2. Plate penetration and density measurements also were made in the test section before traffic. The relations among these measurements for a range of soil strengths are shown in tables 3 and 4.

Traffic application

21. The test carriage towed the test tire through the test section at a constant speed of approximately 1.0 fps. A test consisted of 10 consecutive passes of the tire in the same direction along the same path.

Types of data obtained

22. In a normal test run, performance data were recorded on direct-writing oscillographs during the first, second, third, fifth, seventh, and tenth passes. The types of data recorded were: tire load, towed force, tire sinkage, deflection gage registration, normal interface stresses, soil mass stresses, carriage position, wheel rotation, and the tire record.

PART III: ANALYSIS OF TEST RESULTS

Data Reduction

23. In the form in which they were first obtained, the data were merely records of the simultaneous measurements, which had to be assembled into a coherent system before the results of a test could be analyzed. At each instant in time, there were data that described the position of the wheel axle along the test course, the angular position of each stress cell relative to the wheel axle, the deflection of the tire at each cell's location, and the vertical movement of the wheel axle relative to the soil surface; these data had to be combined to fix each cell's position in space. Then the cell stress registration that prevailed at a particular time could be associated with the cell's position in space to give one point on an interface stress map. In the reduction of the test data for this study, the shape of the deflected tire cross section was determined at 5-deg intervals of rotation. Then the positions of the stress cells were located on each cross section. From these plots the circumferential positions also could be specified. It should be noted that in the plates which pertain to interface stresses (plates 1-8), the measured normal stresses are plotted in their appropriate positions on the vertical and horizontal projections of the actual contact surface. This method of presenting the data is preferred for several reasons. It is necessary to know only the position of the center of the cell diaphragm and not its exact attitude. This method eliminates the need to measure the "developed" (actual) length of the contact surface. As illustrated in fig. 10, this method can be used to readily determine the position and magnitude of the horizontal and vertical components of the resultant of the normal forces on the wheel in the soil. In addition, presenting the stress data in this form facilitates comparisons between the measured data and the stresses theorized by Bernstein, Bekker, and other experimenters who base their theories, in part, on the pressure-sinkage relations obtained during plate-penetration tests. Also, it is thought that the data when analyzed in this fashion have greater utility in the development of theoretical concepts.

STEP 1. DETERMINATION OF EFFECTIVE WIDTH

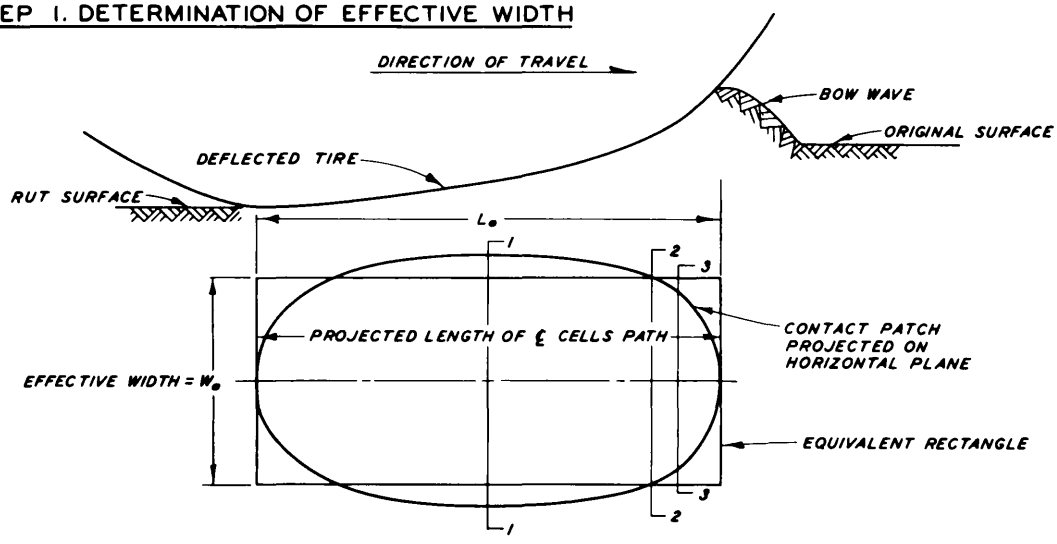

STEP 2. DETERMINATION OF AVERAGE σ_{NZ}'S FOR CROSS SECTIONS

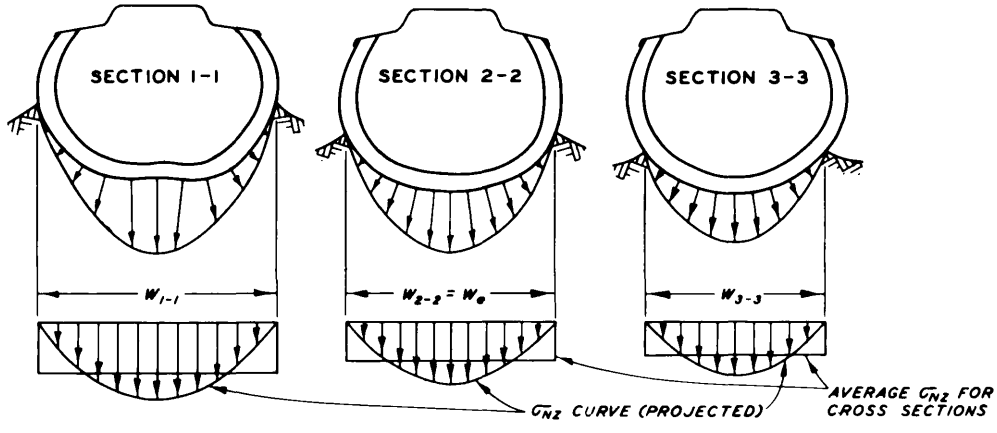

STEP 3. DETERMINATION OF AVERAGE σ_{NZ}'S FOR CONTACT AREA

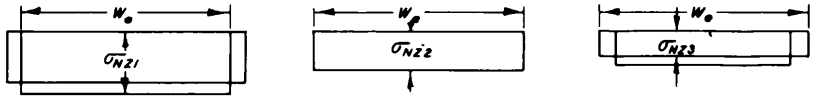

STEP 4. AVERAGE STRESS WAVE AND F_Z

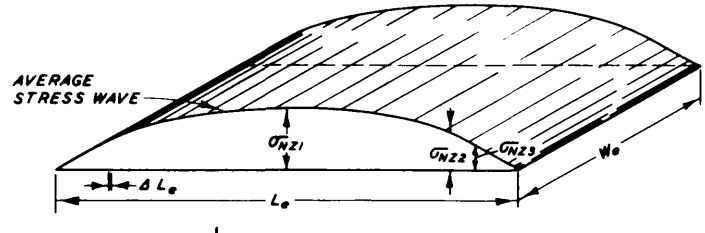

$F_Z = \sum \left[(\sigma_{NZ_i})(\Delta L_e)(W_e) \right]_0^{L_e}$ = VOLUME OF FIGURE

Fig. 10. Steps in determining average stress wave and F_Z

Interface Stresses

24. Plates 1-4 show typical stress maps developed from the test data. The outline(s) of the three-dimensional curved contact surface(s) has been projected onto the horizontal and vertical planes. Since the cells in the tire register stresses (in psi) normal to their diaphragms, the projected stress distributions are obtained merely by locating the centers of the cells on the appropriate projection and plotting the accompanying measured stress magnitudes at those points. Plates 1 and 2 show the distribution of interface stresses for the 11.00-20, 12-PR tire with 3000-lb load at 15-psi inflation pressure on a soft sand. Plates 3 and 4 represent the same test conditions except for the inflation pressure, which was 60 psi.

Effect of inflation pressure

25. In the study of interface stresses on an unyielding surface[4] it was found that relatively high normal stresses, termed edge stresses, existed in a zone near the sides of the contact area elongated parallel to the travel direction. In general, for a constant tire load the intensity of these edge stresses was greatest when the inflation pressure was the lowest; at high inflation pressures the edge stresses were not evident. From plates 1-4 of this report it can be seen that similar trends occur for normal stresses measured in sand. For example, plate 1 depicts a test on loose, soft sand at a 15-psi inflation pressure, and it shows an elongated zone of high stresses offset from the center line of the contact area. Plate 3 depicts a second test on loose sand at a 60-psi inflation pressure, and a similar zone of high stresses offset from the center line does not occur; instead, the stresses increase to a maximum at the center line.

Effect of soil strength

26. Another interesting observation that can be made from these tests is that the surface strength influences the development of the stress patterns. Plate 5 compares the interface stresses recorded during two tests in sand of different strength at a single (15 psi) inflation pressure. Plate 6 compares two extreme conditions, a tire operating at 15 psi on an unyielding surface and on a soft sand. All of the curves in plates 5 and 6 have been somewhat smoothed and idealized to aid in the comparison.

Only a cross section at the axle and a center-line registration (profile) are shown for clarity. It can be seen that in the central portion of the contact width the stresses are not widely different in magnitude. The distribution patterns along the profile also are seen to be similar; however, the contact length (profile) is longer in the soft sand. A marked difference in peak or maximum stresses is evident in the cross-section comparison shown. On the unyielding surface, very high stresses are concentrated near the edge of the tire contact. On the yielding sand, these edge stresses are much smaller, being a minimum for the soft (30 CI) sand, and overall the stresses are distributed to portions of the tire farther from the center line of the cross section.

Effect of tire deflection

27. Plates 7 and 8 illustrate three general types of stress waves that were distinguished in the test results. In each plate are shown the stress registrations at the center line of the tire and at an offset distance of 3.75 in. from the center line on the first pass of the wheel. The offset cell was chosen to indicate the pattern of the edge stresses. The drawings of the deflected tire and the soil surfaces as shown in these plates refer only to the center-line cell position. The circumference of the tire and soil surfaces are not shown for the offset cell position; however, the relative locations of the stress patterns on the projections are correct.

28. The stress patterns shown in plate 7 are typical of those from tests in which the maximum in-soil tire deflections (δ_{MS}) were small, usually less than about 10 percent. These patterns can be identified both by the single-peaked curves at the center line and at the offset and by the greater pressure on the center line (point for point) than on any other parallel line. Tests in which δ_{MS} was greater than about 10 percent usually furnished stress curves of the type shown in plate 8. For these tests, the center-line cell always exhibited two maxima in the stress wave. The cell at the 3.75-in. offset was single-peaked, and the high stress occurred at the same cross section at which the minimum stress between the two peaks of the center-line stress wave occurred. Thus, the latter stress patterns are those in which the edge stresses tend to predominate.

Approximation of stress patterns

29. Average stress wave. Stress maps of the type illustrated in plates 1-4 provide a graphic means of studying the general nature of the stress distribution patterns. However, they do not lend themselves readily to mathematical manipulation. In an effort to provide a basis on which to analyze data mathematically, the concept of an average stress wave has been introduced. The concept also permits determination of total forces on the wheel without the necessity of laborious planimetering of areas.

30. Averaging procedure. The average stress waves, which are plotted on the major axes of the projected (vertical and horizontal) contact areas, represent, at any point, the average stress over the average width (termed effective width, W_e) of the pertinent cross section. The steps employed in constructing an average stress wave projected in a horizontal plane (i.e. vertical stresses) are described in the following example (refer to fig. 10, p 26). Horizontal stresses are determined in a similar manner.

Step 1. The outline of the actual area of contact between tire and soil is projected onto the horizontal plane. The projected length of the contact patch is the projected length of the path followed by a cell embedded in the center line of the tire while in contact with the soil. The projected widths are approximated by constructing the cross section of the tire at various angular positions (from deflection gage data) at the proper depths (from sinkage data) in the soil. The bow wave is taken into consideration. A rectangle equal in area and in length to the contact area (projected) is drawn. The width of this rectangle is termed effective width (W_e). This step is illustrated in fig. 10 for three cross sections, 1-1, 2-2, and 3-3, with projected widths greater than, equal to, and less than the effective width, respectively.

Step 2. The average normal stress projected on a horizontal plane (σ_{nz}) for a particular cross section is determined by drawing a rectangle in which the length is equal to the projected width of the tire cross section and the area is equal to the area under the σ_{nz} curve. The width of this rectangle is

the average σ_{nz} for the respective cross section.

Step 3. The average σ_{nz} for a particular cross section is converted to the average σ_{nz} to be used as a point on the average stress wave by multiplying it by the ratio of the projected width of the cross section to the effective width. This step is illustrated in fig. 10 by construction of a rectangle equal in area to that constructed in step 2, but with a length equal to W_e. The width of this rectangle is then the proper value of σ_{nz} for constructing the average stress wave, which is shown in step 4.

31. Determination of location and magnitude of vertical force. When the proper values for σ_{nz} have been computed, the average stress wave can be constructed (see step 4, fig. 10). To compute the vertical force (F_z) the stress wave is first divided into even increments (ΔL_e), the average stress on each increment being also the average stress for the cross section represented at the midpoint of that increment; therefore,

$$F_z = \sum \left[(\sigma_{nzi})(\Delta L_e)(W_e) \right]_0^{L_e}$$

where

σ_{nz} = psi
ΔL_e = in.
W_e = in.

The location of the line of action of F_z was usually determined by taking moments about point 0 (see step 4, fig. 10). Obviously, the location and magnitude of F_x can be determined in a similar manner. Actual and computed values for eight representative tests are shown in the following tabulation. The results indicate that the methods used were reasonable.

Avg 0- to 6-in. Cone Index	Inflation Pressure psi	Applied Wheel Load lb	Measured Towing Force lb	Computed		% Difference (i.e. $\frac{\text{Computed - Actual}}{\text{Actual}} \times 100$)	
				Wheel Load lb	Towing Force lb	Wheel Load	Towing Force
16	15	3000	870	2950	862	-1.7	-0.9
15	30	3000	1028	2961	1098	-1.3	6.8
16	60	3000	1115	2914	1142	-2.9	2.4
24	15	3000	760	3230	703	7.7	-7.5
30	15	3000	609	3104	563	3.5	-7.6
27	60	3000	1000	3032	1124	1.1	12.4
57	15	3000	166	3130	187	4.3	12.7
54	60	3000	943	3147	1083	4.9	14.8

32. Fourier series approximation. The average stress waves can be expressed mathematically in terms of a Fourier series (see Appendix A). Established mathematical techniques are used to develop an integrable equation of the form

$$f(x) = \sum_{n=1}^{\infty} (a_n \sin nx)$$

where $f(x)$ for purposes of this discussion can be considered to be the stress at any point x. The coefficients a_n are the necessary constants for the n terms of the series and can be assumed to be dependent upon the test conditions. Theoretically an infinite number of components are required to exactly duplicate the stress wave, but it has been found that even the most complex of the stress waves obtained in this study could be closely approximated by a Fourier series with 19 harmonics (plate 9). The general shape of most curves could be obtained with as few as three or four harmonics (plate 10).

33. The coefficients (expressed as a decimal fraction of the maximum ordinate of the stress wave) of the first seven terms of the Fourier series approximations of a number of average stress waves (projected on the horizontal plane) are listed in table 5. An examination of these data shows that in most cases the even-numbered coefficients are quite small. The first coefficient is quite large, and there is a tendency for the fractional value to be less than unity for single-peaked curves and greater than unity for the double-peaked curves. Test 34 is an exception to this rule, however. This test was run on a rather firm sand at a relatively low inflation pressure, and the large maximum stress that resulted shows a trend toward the high stress levels that occur on unyielding surfaces under similar test conditions. The values of the maximum ordinates in this series of tests seem to show a relation to the test inflation pressure (i.e. the higher the inflation pressure, the greater the ordinate value), again with the exception of test 34. When further data become available, trends in the Fourier coefficients in terms of loads, inflation pressures, and soil strengths will be explored.

Location of resultant forces

34. The tests analyzed in this report were conducted with a freely

rolling (towed) wheel. For this condition, the only moment about the wheel axle is that caused by friction in the bearings. If this frictional moment is neglected, the conditions of static equilibrium require that the resultant of all forces pass through the axle center line so that no net moment exists. However, besides the normal stresses that are measured by the stress cells, the possibility of stresses tangential to the tire surface exists. Although the tangential stresses could not be measured directly with the presently available instrumentation, their net magnitude can be estimated from the residual moment, if any, of the resultant of the normal stresses (see fig. 11).

35. Computations using the data from the tests reported herein indicate that the resultant of the normal stresses at the tire-soil interface probably intersects the axle center line. The basis for these computations is outlined schematically in fig. 11. To compute the direction and magnitude of the resultant of the normal stresses (F_r), the magnitude and location of the resultants of the projected normal stress distributions (F_x for the horizontal projection, F_z for the vertical projection) were determined. Then the point of intersection of F_x and F_z and the magnitude and line of action of F_r were computed. Of 17 tests analyzed, the resultant normal force always passed forward and within 0.5 in. of the axle center line. In only four instances was the distance, a (see fig. 11), more than 0.2 in. The tests in which the resultant had the greatest departures from the axle were those tests at deflections of 25 percent or greater. Thus it can be concluded that the normal stresses do not produce a moment about the axle. This requires that the resultant of the tangential stresses, τ, be zero to produce a balanced moment equation. However, negative slip is known to occur in a towed test, and slip must be accompanied by some tangential force. Therefore, another tangential force acting in the direction opposite to that of the slip-induced force must be set up at the interface. Probably this counterbalancing force arises from the flow of sand in front of the tire as evidenced by the formation of the bow wave. Further studies, preferably employing a tangential stress cell if one can be developed, are needed to clarify these observations.

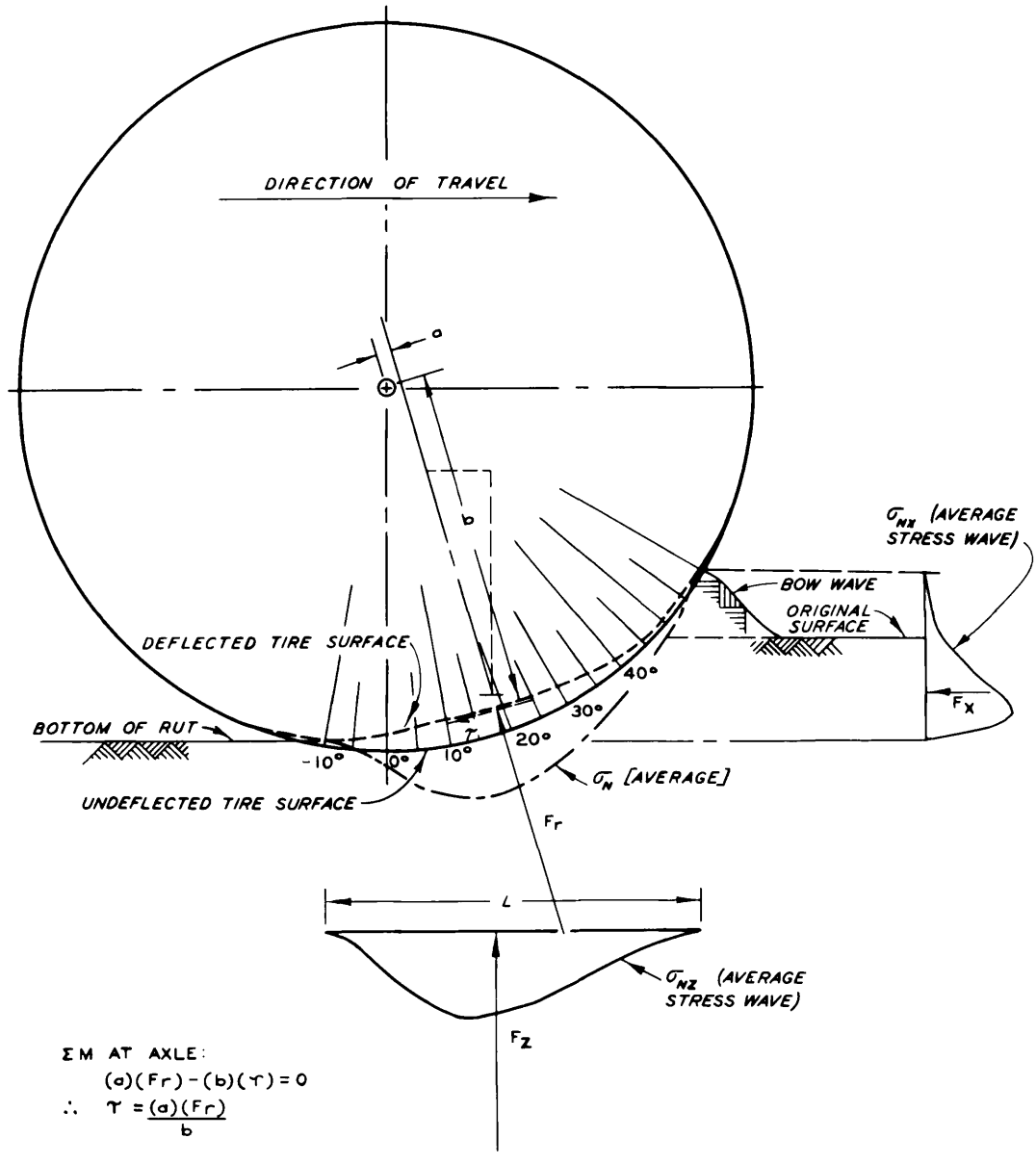

Fig. 11. Normal and tangential forces on a towed pneumatic tire in soft soils

Comparison of pressure-sinkage relations for a tire and a plate

36. Previous attempts have been made by WES and others, mainly the Land Locomotion Laboratory, to describe the pressure-sinkage relation for a moving tire in the same terms as for a flat plate pushed vertically into a

soil. The latter relation, known as the Bernstein equation, takes the form $p = Kz^n$ where p is pressure on the plate, z is sinkage, and K and n are constants. Until the studies reported herein were made, no reliable pressure-sinkage data for a tire were available to compare with similar data for a plate. Plate 11 shows a pressure-sinkage relation from a typical average stress curve with a superimposed pressure-sinkage curve from a plate-penetration test in the same soil. At the intermediate depths, the magnitude of the pressure from both sources is about the same. However, the plate test fails to indicate a decrease in pressure similar to that experienced by the tire near the maximum penetration; and the plate test could not, of course, measure anything analogous to the bow wave effects. Furthermore, in some of the tire tests in this study, the pressure-sinkage relation for the tire had a double-peaked pattern (see plate 8), and it seems unlikely that a plate test would show a similar phenomenon. "While these results do not prove the Bernstein equation invalid, it does convincingly demonstrate that if the equation does have an application in wheel mobility work, it must be applied with more finesse than has been used to date. On the other hand, it cannot be reported yet that the pressure-distribution studies have resulted in a broad new working hypotheesis. The data show that the problem is quite complicated and that consideration may also have to be given such things as relative slip and tire construction. However, the data do suggest that there may be simplifying assumptions that can be made with a reasonable degree of validity that could allow a general hypothesis to be made eventually. This is one of the goals of this research, and a solid effort will be made to reach it."[5]

Stresses in the Soil Mass

Position of maximum stress

37. The maximum stress registered by the cells buried in the sand tended to occur before the axle of the rolling tire passed over the cell location. However, well-defined maxima usually occurred only when the test conditions were such that single-peaked stress curves were registered by the stress cells in the tire. In these instances, a definite relation between tire deflection, interface stresses, and stresses in the soil mass

could be observed. An example is shown in plate 12. The maximum tire deflection and the maximum interface stress occurred at an angle of 13-1/2 degrees ahead of the axle center line. In other terms, in the particular example shown, the maximum stress in the cell in the soil was registered before the maximum interface stress. The maximum interface stress occurred when the axle had moved forward an additional 0.4 in. Finally, the angle of the measured resultant force in this test was about 18-1/2 degrees. It seems evident that these measurements are interrelated, but further data and analysis are needed before any additional conclusions can be drawn.

Effects of soil strength on stress

38. Several tests in this test program were similar in most respects except for the soil strength. The maximum stresses registered in these tests by the cells in the soil on various passes of the test wheel are plotted in plate 13 and listed in table 6. The spread of data discourages a confident interpretation, but it will be noted that stress values from the test in the sand of highest strength were median between those values recorded for tests in the two sands with lower strength, thus suggesting that the magnitude of the stresses did not vary in a consistent manner with variations in the strength of the sand. The results also imply that the effective modulus of elasticity and Poisson's ratio did not vary widely for the range of soil conditions represented.

Effects of load on stress

39. The test data (table 6) also permit an evaluation of the effects of load on the stresses. This evaluation of the data is shown in plate 14. At any depth, the magnitude of the induced stress is approximately in direct proportion to the magnitude of the applied load. This trend was what had been expected.

PART IV: CONCLUSIONS AND RECOMMENDATIONS

Conclusions

40. On the basis of the data presented in this report, it is concluded that:

a. The equipment, facilities, and techniques employed in these tests produce a reasonably correct portrayal of the distribution of normal stresses at the tire-soil interface.

b. The Fourier series description of average stress curves shows promise as a means of describing and manipulating the measured stress patterns.

c. Within the probable accuracy of the analysis of the data as reported herein, the line of action of resultant of the normal stresses at the tire-soil interface can be considered to pass through the wheel axle center line of tires towed in sand.

d. The average pressure-sinkage relation for a pneumatic tire towed in sand is not approximated closely by an average pressure-sinkage relation from a plate-penetration test.

e. The magnitudes of the stresses induced in sand by a moving tire are influenced by the load on the tire (i.e. the greater the load, the greater the stress). No consistent influence of the relative firmness of the sand on stress magnitudes was observed.

f. The maximum induced stress registered by a cell embedded in the soil mass during passage of the wheel occurs before the wheel reaches a position over the cell. The position of the maximum induced stress appears to be related to the stresses and deformations at the tire-soil interface.

Recommendations

40. It is recommended that:

a. This study be extended to include some fundamental tests

with towed wheels in soft clay soils, and powered wheels in both air-dry sand and wet, soft clay soils.

b. An effort be made to develop a cell, suitable for use in pneumatic tires, that will measure tangential stresses.

c. Analyses of the existing data for towed wheels in sand be continued.

LITERATURE CITED

1. U. S. Army Engineer Waterways Experiment Station, CE, Deflection of Moving Tires. Technical Report No. 3-516, Vicksburg, Miss.

   a. Report 1, A Pilot Study on a 12 x 22.5 Tubeless Tire, July 1959.

   b. Report 2, Tests with a 12.00-22.5 Tubeless Tire on Asphaltic Concrete, Sand, and Silt, 1959-1960, August 1961.

   c. Report 3, Center Line Deflection Studies Through July 1963, (in preparation).

2. _____, Stresses Under Moving Vehicles. Vicksburg, Miss.

   a. Report 1, A Pilot Study of WES Earth Pressure Cell Action in Comparatively Soft Soil. Miscellaneous Paper No. 4-230, July 1957.

   b. Report 2, Wheeled Vehicles (M135), Lean and Fat Clay, 1957. Technical Report No. 3-545, May 1960.

   c. Report 3, Tracked Vehicles (M29C, D4, and D7) on Fat Clay, 1956. Technical Report No. 3-545, July 1960.

   d. Report 4, Distribution of Stresses on an Unyielding Surface Beneath Stationary and Towed Pneumatic Tires. Technical Report No. 3-545, July 1964.

3. _____, Tests with Rigid Wheels; Tests in Fat Clay, 1958. Technical Report No. 3-565, Report 1, Vicksburg, Miss., May 1961.

4. Freitag, D. R., and Green, A. J., "Distribution of stresses on an unyielding surface beneath a pneumatic tire." Stress Distribution in Earth Masses, Bulletin 342, Highway Research Board, Washington, D. C. (1962), pp 14-23.

5. U. S. Army Engineer Waterways Experiment Station, CE, Comments on Mobility Research, by S. J. Knight. Miscellaneous Paper No. 4-623, Vicksburg, Miss., February 1964.

Table 1

Hard-Surface Deflections, Contact-Print Dimensions, and Average Contact Pressure

11.00-20, 12-PR Tire, Buffed Smooth

Wheel Load lb	Inflation Pressure psi	Maximum Hard-Surface Deflection in.	Maximum Hard-Surface Deflection %	Contact-Print Dimensions Length in.	Contact-Print Dimensions Width in.	Contact-Print Dimensions Area sq in.	Average Contact Pressure psi
4500	60	1.56	17.3	11.35	6.38	67	67
4500	30	2.22	24.6	16.00	8.20	125	36
4500	15	5.00	55.4	20.00	9.30	187	24
3000	60	1.12	12.5	9.90	6.05	52	58
3000	30	1.75	19.4	12.38	7.40	86	35
3000	15	2.75	30.4	16.10	8.20	130	23
1500	60	0.50	5.5	7.70	4.60	29	51
1500	30	0.88	9.7	9.90	5.65	47	32
1500	15	1.31	13.1	10.50	6.65	62	24

Table 2

Cone Index Data

Mortar Sand Test Section

Test No.	Load lb	Inflation Pressure psi	Depth Range in.	Cone Index Before Indicated Pass 1	2	3	5	7	10
3	3000	60	0-6	23	24	24	--	--	--
			6-12	85	90	92	--	--	--
4B	4500	60	0-6	27	21	28	32	35	37
			6-12	108	104	--	--	--	--
5A	1500	15	0-6	28	20	22	27	31	30
			6-12	116	81	82	97	104	107
6	1500	30	0-6	25	26	31	31	31	33
			6-12	120	87	98	97	92	100
7	1500	60	0-6	26	26	30	31	34	40
			6-12	121	101	101	105	119	141
8	3000	15	0-6	25	20	25	29	30	33
			6-12	146	92	103	112	111	119
9	3000	30	0-6	27	22	28	29	30	34
			6-12	113	93	115	120	123	139
10	4500	15	0-6	28	28	20	23	24	28
			6-12	102	67	75	84	93	108
11	4500	30	0-6	29	20	24	27	25	26
			6-12	99	70	86	96	97	98
12	3000	30	0-6	43	24	24	30	31	32
			6-12	154	111	102	125	125	130
12A	3000	30	0-6	55	25	26	29	31	35
			6-12	205	109	113	119	133	148
13	3000	60	0-6	57	29	31	31	32	33
			6-12	208	130	131	131	137	143
14	4500	30	0-6	60	27	27	34	36	40
			6-12	272	142	140	150	156	165
15	--	--	0-6	--	--	--	--	--	--
			6-12	--	--	--	--	--	--
16	4500	15	0-6	60	27	26	30	32	36
			6-12	146	83	84	110	125	124
17	1500	60	0-6	62	28	30	35	39	46
			6-12	150	100	111	137	149	136
18	1500	30	0-6	59	24	26	32	37	41
			6-12	174	89	113	125	138	131

(Continued)

Table 2 (Concluded)

Test No.	Load lb	Inflation Pressure psi	Depth Range in.	Cone Index Before Indicated Pass					
				1	2	3	5	7	10
19	3000	15	0-6	58	29	34	30	32	36
			6-12	233	118	132	125	121	142
20	4500	60	0-6	57	28	29	30	32	35
			6-12	192	130	137	--	--	--
21	1500	15	0-6	63	29	30	32	35	39
			6-12	235	123	126	124	132	145
22	1500	15	0-6	18	17	24	34	39	40
			6-12	47	73	96	123	149	156
23	1500	30	0-6	14	16	23	33	34	42
			6-12	39	67	92	119	134	146
24	1500	60	0-6	16	18	23	32	36	39
			6-12	49	74	98	121	130	141
25	3000	15	0-6	19	21	28	33	38	41
			6-12	50	81	106	124	154	154
26	3000	30	0-6	15	17	24	32	36	42
			6-12	36	74	76	129	143	171
27	3000	60	0-6	16	17	22	29	33	36
			6-12	49	69	93	--	--	--
28	4500	60	0-6	17	17	22	29	34	38
			6-12	54	75	102	125	--	--
29	4500	30	0-6	17	19	30	36	41	43
			6-12	65	73	103	129	149	158
30	4500	15	0-6	17	22	27	31	34	37
			6-12	53	74	93	111	122	138
31	3000	60	0-6	27	20	25	32	41	41
			6-12	94	83	106	128	150	150
32	3000	15	0-6	24	25	29	34	37	39
			6-12	77	88	100	115	124	134
33	3000	60	0-6	54	25	28	33	35	38
			6-12	168	124	138	156	165	175
34	3000	15	0-6	57	29	28	28	29	32
			6-12	232	129	125	136	151	169
35	3000	15	0-6	30	21	25	30	32	34
			6-12	140	85	103	130	143	155
200	4500	60	0-6	84	32	31	29	31	35
			6-12	320	131	150	161	--	--
201	1500	15	0-6	79	39	35	36	37	40
			6-12	--	170	168	156	166	183

Table 3

Plate Penetration Data

Mortar Sand Test Section

0- to 6-in. Layer Cone Index	Depth in.	Plate Penetration Resistance, psi 1.4-in.-diam plate	2.8-in.-diam plate	4.2-in.-diam plate
15-17	0.25	1.7	2.5	2.0
	0.50	2.4	3.2	3.0
	0.75	3.2	3.6	3.7
	1.00	4.0	3.9	4.2
	1.50	5.7	4.7	5.3
	2.00	7.0	5.9	6.1
	3.00	9.8	7.8	8.0
	4.00	12.1	9.9	10.0
	5.00	14.2	12.9	12.0
	6.00	16.2	14.1	13.8
	7.00	18.1	16.1	16.4
	8.00	19.8	18.5	18.6
25-30	0.25	5.5	6.3	7.0
	0-50	9.0	11.0	11.5
	0.75	10.0	12.0	13.0
	1.00	11.0	12.8	13.7
	1.50	16.2	16.6	15.5
	2.00	20.4	17.9	17.3
	3.00	29.0	22.7	21.3
	4.00	37.0	28.6	25.6
	5.00	45.0	34.0	33.2
	6.00	53.0	39.5	37.2
	7.00	60.0	43.8	40.8
	8.00	67.0	48.2	44.4
55-60	0.25	5.8	12.2	15.7
	0.50	10.4	15.9	23.6
	0.75	14.3	17.9	23.9
	1.00	18.2	19.5	24.0
	1.50	26.0	26.0	26.9
	2.00	35.0	33.3	30.5
	3.00	52.0	45.0	38.0
	4.00	69.0	56.5	46.0

Note: These data are averages for each cone index range.

Table 4

Average Density-Cone Index Data

Mortar Sand Test Section

Cone Index 0- to 6-in. Layer	Dry Density* (γ_D) in lb/cu ft 0- to 3-in. Layer
15	95.1
20	96.0
25	96.8
30	97.7
35	98.5
40	99.2
45	99.9
50	100.6
55	101.2
60	101.8

* Values taken from curves based on a number of tests.

Table 5

Fourier Coefficients of Average Stress Waves

Test No.	Load lb	Inflation Pressure psi	Max In-Soil Deflection %	Sinkage z in.	Towed Force P_T lb	Cone Index 0- to 6-in. Layer	Max Ordinate of Stress Wave psi	Fourier Coefficients* for Indicated Sine Terms							Type of Avg Curve**
								1	2	3	4	5	6	7	
25	3000	15	19.5	3.92	870	16	18.0	1.12	0.08	0.10	0.04	-0.03	-0.00	-0.02	Flat
26	3000	30	7.8	5.64	1040	15	25.6	0.98	0.08	-0.05	-0.05	0.00	-0.02	0.00	Single
27	3000	60	4.6	6.74	1105	16	33.0	0.82	0.11	-0.06	-0.05	-0.06	0.00	0.01	Single
31	3000	60	5.0	5.65	1000	27	26.5	0.92	0.06	-0.09	-0.04	-0.05	-0.01	-0.01	Single
32	3000	15	22.2	3.21	750	24	18.2	1.03	0.01	0.35	-0.02	0.10	-0.06	0.05	Double
33	3000	60	6.1	3.64	825	55	33.0	0.93	0.07	-0.07	0.02	-0.01	-0.01	0.00	Single
34	3000	15	27.8	0.29	225	57	29.1	0.67	0.01	0.42	0.10	0.21	0.05	0.06	Double
35	3000	15	25.6	2.41	615	30	18.0	1.10	0.00	0.15	-0.01	-0.07	-0.05	-0.02	Double

* Expressed as decimal fraction of maximum ordinate of stress wave.

** Single-peak stress wave; flat (single) peak stress wave; double-peak stress wave.

Table 6

Stresses in the Soil Mass, Mortar Sand

11.00-20, 12-PR Smooth Tire

Pass	Cell No. 1 Peak Station No.	Cell No. 1 Peak Pressure psi	Cell No. 1 Vertical Pressure psi	Cell No. 2 Peak Station No.	Cell No. 2 Peak Pressure psi	Cell No. 2 Vertical Pressure psi	Cell No. 3 Peak Station No.	Cell No. 3 Peak Pressure psi	Cell No. 3 Vertical Pressure psi	Average Depth in.	Average Peak Pressure psi	Average Vertical Pressure psi
						Test 16						
1				59.58	9.4	9.2	62.58	8.1	8.0	17.5	8.75	8.60
2				59.60	9.1	8.9	62.59	8.0	7.9	17.1	8.55	8.40
3	Cell 1 out of operation			59.60	9.1	8.9	62.58	8.0	7.9	16.8	8.55	8.40
5				59.64	9.3	8.9	62.62	8.2	7.9	16.3	8.75	8.40
7				59.67	9.2	8.8	62.63	8.1	7.9	16.0	8.65	8.35
10				59.70	9.5	9.0	62.64	8.3	8.0	15.6	8.90	8.50
						Test 17						
1				59.40	3.0	2.8	62.40	2.5	2.4	17.1	2.75	2.60
2				59.33	2.5	2.2	62.30	2.1	2.0	16.5	2.30	2.10
3	Cell 1 out of operation			59.34	2.5	2.2	62.30	2.3	2.0	16.1	2.40	2.10
5				59.40	2.3	2.2	62.41	2.2	2.1	15.8	2.25	2.15
7				59.41	2.3	2.2	62.35	2.2	2.1	15.6	2.25	2.15
10				59.50	2.3	2.3	62.47	2.2	2.1	15.4	2.25	2.20
						Test 18						
1	56.40	2.8	2.8	59.33	2.2	2.1	62.23	2.2	2.0	17.1	2.40	2.30
2	56.44	2.9	2.8	59.32	2.0	1.8	62.20	2.2	1.9	16.4	2.36	2.16
3	56.52	3.0	2.9	59.37	2.1	2.0	62.30	2.2	1.9	16.1	2.43	2.26
5	56.49	3.2	3.2	59.41	2.1	2.1	62.37	2.3	2.2	15.7	2.53	2.50
7	56.52	3.5	3.5	59.40	2.1	2.1	62.36	2.3	2.1	15.5	2.63	2.56
10	56.43	3.5	3.5	59.48	2.3	2.3	62.40	2.4	2.4	15.4	2.73	2.73
						Test 19						
1	56.76	7.1	6.8	59.50	5.1	5.0	62.56	4.8	4.8	17.7	5.66	5.53
2	56.74	6.9	6.4	59.58	4.7	4.5	62.57	4.5	4.4	17.4	5.36	5.10
3	56.73	7.2	6.9	59.61	4.5	4.1	62.59	4.6	4.5	17.3	5.43	5.16
5	56.78	7.1	6.5	59.58	4.8	4.6	62.59	4.9	4.8	16.9	5.60	5.30
7	56.78	7.0	6.2	59.65	4.5	4.4	62.57	4.8	4.8	16.7	5.43	5.13
10	56.79	6.9	6.0	59.61	4.9	4.8	62.60	4.8	4.8	16.4	5.53	5.20
						Test 20						
1	56.09	13.0	8.6	59.02	7.1	4.3	62.02	6.8	4.2	14.8	8.96	5.70
2	56.04	15.1	9.2	59.10	7.0	4.3	62.09	6.5	4.5	14.0	9.53	6.00
3	56.07	16.6	9.6	59.06	7.1	4.2	62.09	6.4	4.0	13.4	10.03	5.93
5	56.14	18.5	11.1	59.14	7.1	4.6	62.10	6.2	4.0	12.6	10.60	6.56
7	56.20	18.1	13.5	59.17	7.0	4.8	62.13	7.2	4.4	12.3	10.76	7.56
10	56.25	19.6	15.9	59.24	7.1	6.5	62.23	7.3	5.8	12.1	11.33	9.40
						Test 21						
1	57.13	2.6	1.5	60.14	2.9	1.2	63.16	2.9	1.2	17.6	2.80	1.30
2	57.18	2.3	1.7	60.13	2.5	1.4	63.17	2.6	1.3	17.4	2.46	1.46
3	57.17	2.3	1.4	60.14	2.3	1.2	63.15	2.5	1.4	17.3	2.36	1.33
5	57.20	2.4	1.3	60.15	2.4	1.3	63.15	2.8	1.5	16.9	2.53	1.36
7	57.22	2.5	1.4	60.18	2.3	1.2	63.15	2.5	1.5	16.8	2.43	1.36
10	57.21	2.2	1.3	60.17	2.2	1.3	63.17	2.6	1.5	16.6	2.33	1.36
						Test 22						
1	57.68	2.9	1.8	60.70	3.0	1.5	63.68	3.1	1.5	14.9	3.00	1.60
2	56.98	3.9	3.8	59.98	4.0	3.9	62.93	3.6	3.5	14.5	3.83	3.73
3	57.12	4.2	4.0	60.06	4.0	3.9	63.01	3.5	3.5	14.4	3.90	3.80
5	57.16	4.2	4.0	60.11	4.0	3.9	63.04	3.6	3.5	14.3	3.93	3.80
7	57.17	4.0	3.8	60.15	3.9	3.8	63.14	3.5	3.4	14.2	3.80	3.66
10	57.22	3.7	3.5	60.18	3.6	3.2	63.11	3.5	3.2	14.2	3.60	3.30

(Continued)

Note: Vertical pressure is the value recorded when the axle of the test wheel was directly above the cell. For tests 16-21 the station numbers of cells 1, 2, and 3 are 56.5, 59.5, and 62.5, respectively; for tests 22-35 the station numbers of cells 1, 2, and 3 are 57, 60, and 63, respectively. (1 of 3 sheets)

Table 6 (Continued)

Pass	Cell No. 1 Peak Station No.	Cell No. 1 Peak Pressure psi	Cell No. 1 Vertical Pressure psi	Cell No. 2 Peak Station No.	Cell No. 2 Peak Pressure psi	Cell No. 2 Vertical Pressure psi	Cell No. 3 Peak Station No.	Cell No. 3 Peak Pressure psi	Cell No. 3 Vertical Pressure psi	Average Depth in.	Average Peak Pressure psi	Average Vertical Pressure psi
						Test 23						
1	56.63	3.1	2.0	59.67	2.2	1.6	62.63	2.0	1.5	14.6	2.43	1.70
2	56.90	3.6	3.4	59.94	2.3	2.1	62.92	2.2	2.0	14.0	2.70	2.50
3	57.03	4.0	3.9	60.07	2.8	2.6	63.05	2.8	2.4	13.9	3.20	2.96
5	57.12	4.8	4.3	60.11	2.6	2.5	63.07	2.5	2.2	13.8	3.30	3.00
7	57.14	4.8	4.4	60.16	2.5	2.2	63.12	2.2	2.1	13.8	3.16	2.90
10	57.23	4.5	4.2	60.24	2.2	2.0	63.17	2.1	2.0	13.7	2.93	2.73
						Test 24						
1	56.54	2.7	1.6	59.59	2.5	1.7	62.64	2.9	1.9	14.8	2.70	1.73
2	56.75	2.9	2.5	59.86	2.6	2.2	62.78	2.9	2.5	14.2	2.80	2.40
3	56.92	3.3	3.2	59.95	2.8	2.6	62.88	3.0	2.8	13.9	3.03	2.86
5	57.08	3.8	3.6	60.02	2.9	2.9	63.03	3.1	3.0	13.8	3.26	3.16
7	57.12	3.7	3.5	60.07	2.9	2.8	63.05	2.8	2.8	13.7	3.13	3.03
10	57.12	3.9	3.8	60.11	2.8	2.6	63.09	2.8	2.8	13.65	3.16	3.06
						Test 25						
1	56.78	5.5	5.0	59.76	5.5	4.5	62.80	5.4	4.8	14.5	5.46	4.76
2	57.10	7.3	7.1	60.00	7.2	7.2	63.03	6.4	6.4	14.5	6.96	6.90
3	57.21	8.6	7.9	60.14	7.8	7.4	63.10	6.9	6.8	14.1	7.76	7.36
5	57.28	9.1	7.9	60.17	7.6	6.9	63.16	7.1	6.8	14.0	7.93	7.20
7	57.31	9.1	7.6	60.20	7.4	6.8	63.19	6.9	6.4	13.9	7.80	6.93
10	57.34	8.5	7.0	60.25	7.0	6.2	63.24	6.5	5.8	13.9	7.33	6.33
						Test 26						
1	56.63	6.2	4.5	59.59	6.1	3.7	62.60	6.0	3.8	14.1	6.10	4.00
2	56.83	7.6	7.0	59.77	6.8	5.8	62.78	6.1	5.0	13.3	6.83	5.93
3	56.93	8.4	8.2	59.91	7.5	7.2	62.91	7.2	6.9	12.9	7.70	7.43
5	57.11	10.0	9.8	60.04	8.8	8.8	63.07	7.5	7.4	12.8	8.76	8.66
7	57.15	10.6	9.9	60.11	9.2	9.0	63.11	7.5	7.0	12.7	9.10	8.63
10	57.23	10.6	9.9	60.14	8.8	8.1	63.15	7.1	6.8	12.7	8.83	8.26
						Test 27						
1	56.54	7.0	3.8	59.52	6.9	3.0	62.26	7.4	3.0	13.9	7.10	3.26
2	56.66	8.5	6.2	59.66	7.4	4.9	62.63	7.4	5.0	13.0	7.76	5.36
3	56.71	9.5	7.8	59.76	7.9	6.0	62.73	7.5	5.8	12.6	8.30	6.53
5	56.93	9.8	9.5	59.85	8.5	7.6	62.82	7.6	7.0	12.2	8.63	8.03
7	56.98	10.0	10.0	59.94	8.6	8.5	62.90	8.4	8.0	12.0	9.00	8.83
10	57.07	10.8	10.8	59.99	9.0	9.0	63.00	8.6	8.6	11.9	9.46	9.46
						Test 28						
1	56.64	10.7	6.8	59.48	8.1	3.1	62.43	9.6	4.1	14.3	9.46	4.66
2	56.71	12.2	9.5	59.65	8.5	5.2	62.59	10.7	6.5	13.4	10.46	7.06
3	56.76	14.2	12.1	59.79	10.0	8.0	62.71	10.5	6.9	13.1	11.56	9.00
5	56.79	14.4	13.6	59.88	10.4	9.3	62.80	9.8	8.3	12.7	11.53	10.40
7	56.90	15.1	14.9	59.93	10.1	9.8	62.83	10.8	9.4	12.5	12.00	11.36
10	56.99	16.0	15.9	59.97	11.0	10.9	62.90	11.5	11.0	12.4	12.83	12.60
						Test 29						
1	56.57	10.1	6.9	59.63	8.2	4.7	62.56	8.5	5.2	13.8	8.93	5.60
2	56.88	12.9	12.2	59.89	10.1	9.8	62.88	10.1	9.8	12.9	11.03	10.60
3	57.06	14.8	14.7	60.01	12.6	12.5	63.00	10.5	10.5	12.7	12.63	12.56
5	57.17	16.8	15.9	60.12	13.8	12.9	63.09	11.7	11.3	12.7	14.10	13.36
7	57.23	16.4	15.0	60.16	13.9	12.5	63.17	12.1	11.3	12.6	14.13	12.93
10	57.26	16.6	14.3	60.25	13.4	11.9	63.20	11.8	10.7	12.6	13.93	12.30
						Test 30						
1	57.01	8.5	8.5	59.94	8.1	7.9	62.82	8.0	7.8	14.6	8.20	8.06
2	57.19	10.8	10.2	60.08	10.5	10.3	63.07	9.8	9.6	14.4	10.36	10.03
3	57.27	11.2	9.9	60.14	11.2	10.7	63.11	10.4	10.0	14.2	10.93	10.20
5	57.36	10.9	9.1	60.19	10.9	10.2	63.18	10.3	10.0	14.0	10.70	9.76
7	57.38	10.1	8.6	60.23	11.0	10.2	63.20	10.1	9.6	13.9	10.40	9.46
10	57.41	9.4	7.6	60.26	10.2	9.4	63.24	9.8	9.0	13.9	9.80	8.66

(Continued)

Table 6 (Concluded)

Pass	Cell No. 1 Peak Station No.	Cell No. 1 Peak Pressure psi	Cell No. 1 Vertical Pressure psi	Cell No. 2 Peak Station No.	Cell No. 2 Peak Pressure psi	Cell No. 2 Vertical Pressure psi	Cell No. 3 Peak Station No.	Cell No. 3 Peak Pressure psi	Cell No. 3 Vertical Pressure psi	Average Depth in.	Average Peak Pressure psi	Average Vertical Pressure psi
						Test 31						
1	56.72	5.5	4.2	59.47	5.0	2.3	62.49	5.3	2.9	13.8	5.26	3.13
2	56.78	5.9	5.1	59.66	5.9	3.9	62.62	5.9	4.0	12.8	5.90	4.33
3	56.87	7.0	6.6	59.77	6.3	4.8	62.71	6.5	4.8	12.4	6.60	5.40
5	57.03	7.8	7.6	59.89	6.6	6.0	62.85	6.9	6.3	11.9	7.10	6.63
7	57.10	8.2	8.0	59.96	7.6	7.4	63.01	7.5	7.4	11.6	7.76	7.60
10	57.20	8.9	8.1	60.02	8.6	8.5	63.08	7.6	7.5	11.5	8.36	8.03
						Test 32						
1	57.05	4.2	4.1	59.86	5.8	5.3	62.82	5.2	4.9	14.7	5.06	4.76
2	57.19	7.9	7.4	60.10	6.7	6.3	63.11	6.1	5.9	14.6	6.90	6.53
3	57.23	8.2	7.5	60.17	7.0	6.5	63.14	6.6	6.1	14.5	7.26	6.70
5	57.30	8.3	7.2	60.24	7.1	6.2	63.19	6.6	5.9	14.4	7.33	6.43
7	57.31	8.0	7.0	60.24	6.9	6.1	63.20	6.3	5.8	14.3	7.06	6.30
10	57.36	7.8	6.4	60.25	6.9	6.1	63.25	6.2	5.7	14.2	6.96	6.06
						Test 33						
1	56.87	5.1	4.9	59.70	5.5	4.1	62.69	4.6	3.6	14.9	5.06	4.20
2	56.89	6.0	5.8	59.77	5.6	4.9	62.76	4.7	4.0	14.2	5.43	4.90
3	56.97	6.3	6.2	59.81	5.5	5.1	62.84	5.0	4.8	13.8	5.60	5.36
5	57.06	7.3	7.2	59.88	6.0	5.8	62.85	6.9	5.2	13.4	6.73	6.06
7	57.08	7.5	7.2	59.93	6.8	6.7	62.89	6.3	6.0	13.2	6.86	6.63
10	57.15	8.2	7.9	59.98	6.8	6.7	62.96	6.8	6.6	13.1	7.26	7.06
						Test 34						
1	57.36	5.6	5.1	60.25	5.4	5.2	63.24	5.2	5.0	17.7	5.40	5.10
2	57.33	6.6	5.9	60.24	5.1	4.9	63.20	4.9	4.8	17.5	5.53	5.23
3	57.33	6.3	5.9	60.21	4.9	4.7	63.22	4.9	4.5	17.3	5.36	5.03
5	57.34	6.0	5.3	60.23	4.9	4.8	63.22	5.0	4.9	17.0	5.30	5.00
7	57.37	6.1	5.6	60.25	4.9	4.6	63.25	4.8	4.5	16.7	5.26	4.90
10	57.37	5.1	4.5	60.24	4.8	4.5	63.20	4.8	4.5	16.5	4.90	4.50
						Test 35						
1	57.00	5.8	5.8	59.93	5.6	5.5	62.95	5.5	5.4	15.6	5.63	5.56
2	57.23	6.8	6.2	60.18	5.7	5.4	63.14	6.2	6.0	15.2	6.23	5.86
3	57.28	7.1	6.6	60.23	5.6	5.0	63.18	6.1	5.8	15.0	6.26	5.80
5	57.31	7.1	6.1	60.23	5.6	4.9	63.21	6.2	5.9	14.8	6.30	5.63
7	57.36	7.3	6.5	60.24	5.8	5.1	63.23	6.2	5.8	14.7	6.43	5.80
10	57.38	6.9	6.0	60.29	5.3	4.8	63.30	6.1	5.5	14.5	6.10	5.43

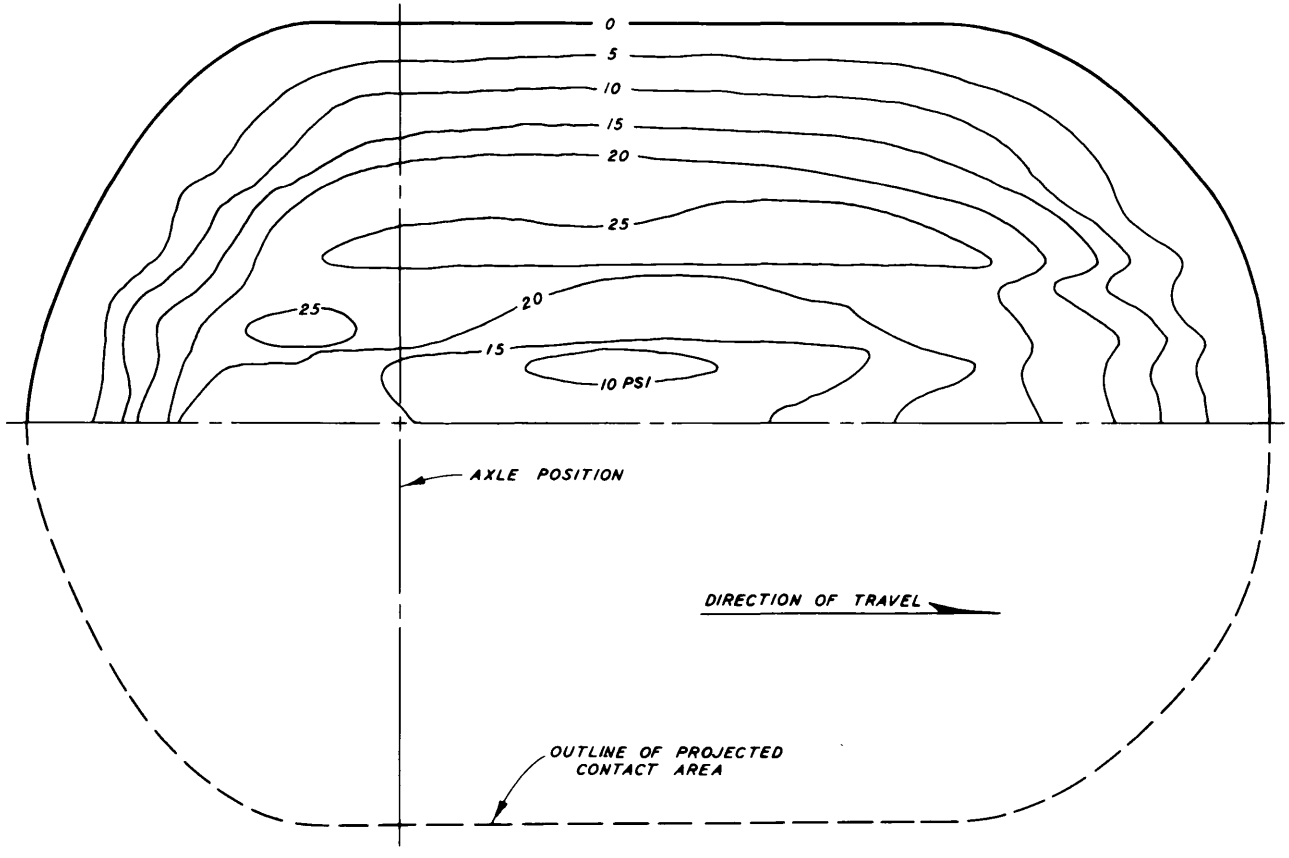

SCALE IN INCHES

1 0 1 2 3

DISTRIBUTION OF NORMAL STRESSES PROJECTED ON HORIZONTAL PLANE

TOWED 11.00-20, 12-PR SMOOTH TIRE
3000-LB LOAD, 15-PSI INFL PRESS.
0- TO 6-IN. CONE INDEX = 30

PLATE 1

PLATE 2

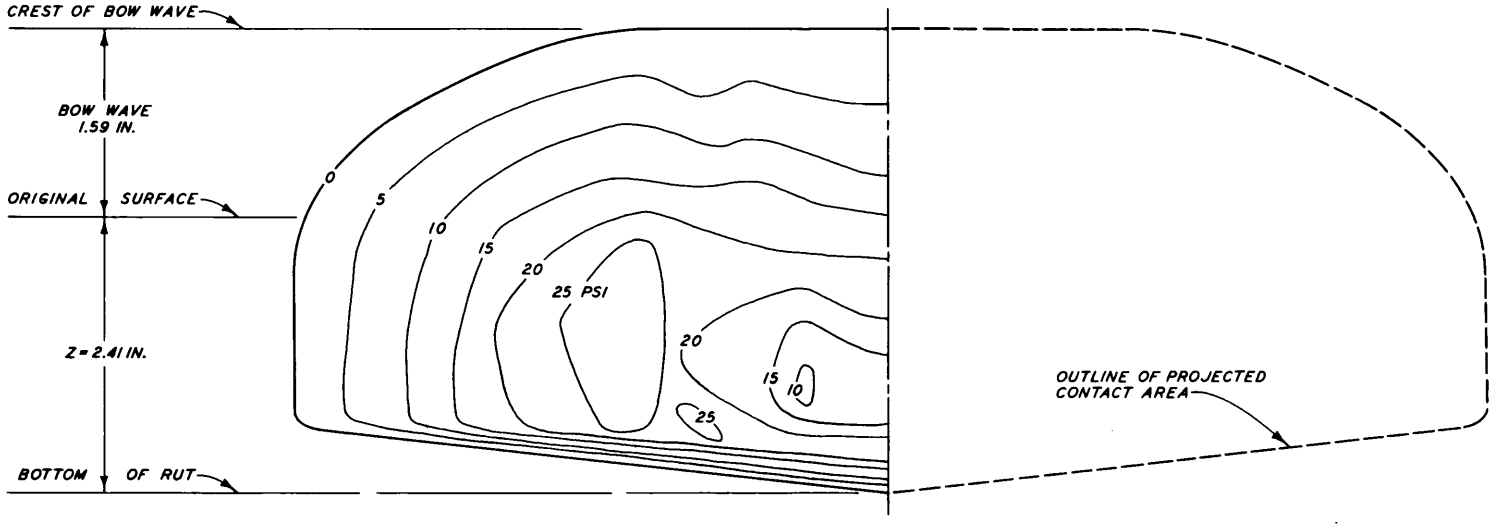

NOTE: DIRECTION OF TRAVEL IS NORMAL TO PLANE OF DRAWING.

SCALE IN INCHES

1 0 1 2

DISTRIBUTION OF NORMAL STRESSES PROJECTED ON VERTICAL PLANE

TOWED 11.00-20, 12-PR SMOOTH TIRE

3000-LB LOAD, 15-PSI INFL PRESS.

0- TO 6-IN. CONE INDEX = 30

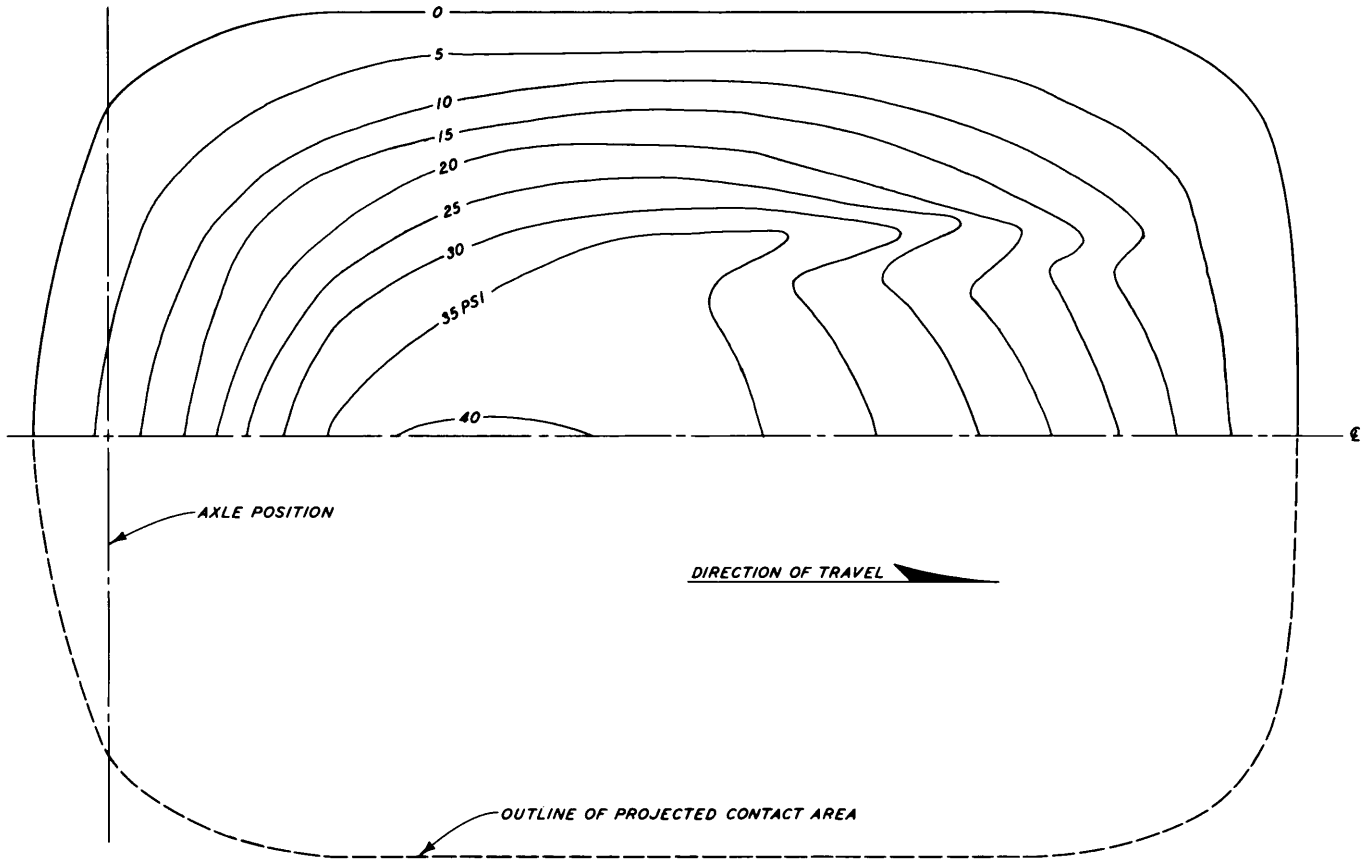

SCALE IN INCHES

1 0 1 2 3 4

DISTRIBUTION OF NORMAL STRESSES PROJECTED ON HORIZONTAL PLANE

TOWED 11.00-20, 12-PR SMOOTH TIRE

3000-LB LOAD, 60-PSI INFL PRESS.

0- TO 6-IN. CONE INDEX = 27

PLATE 3

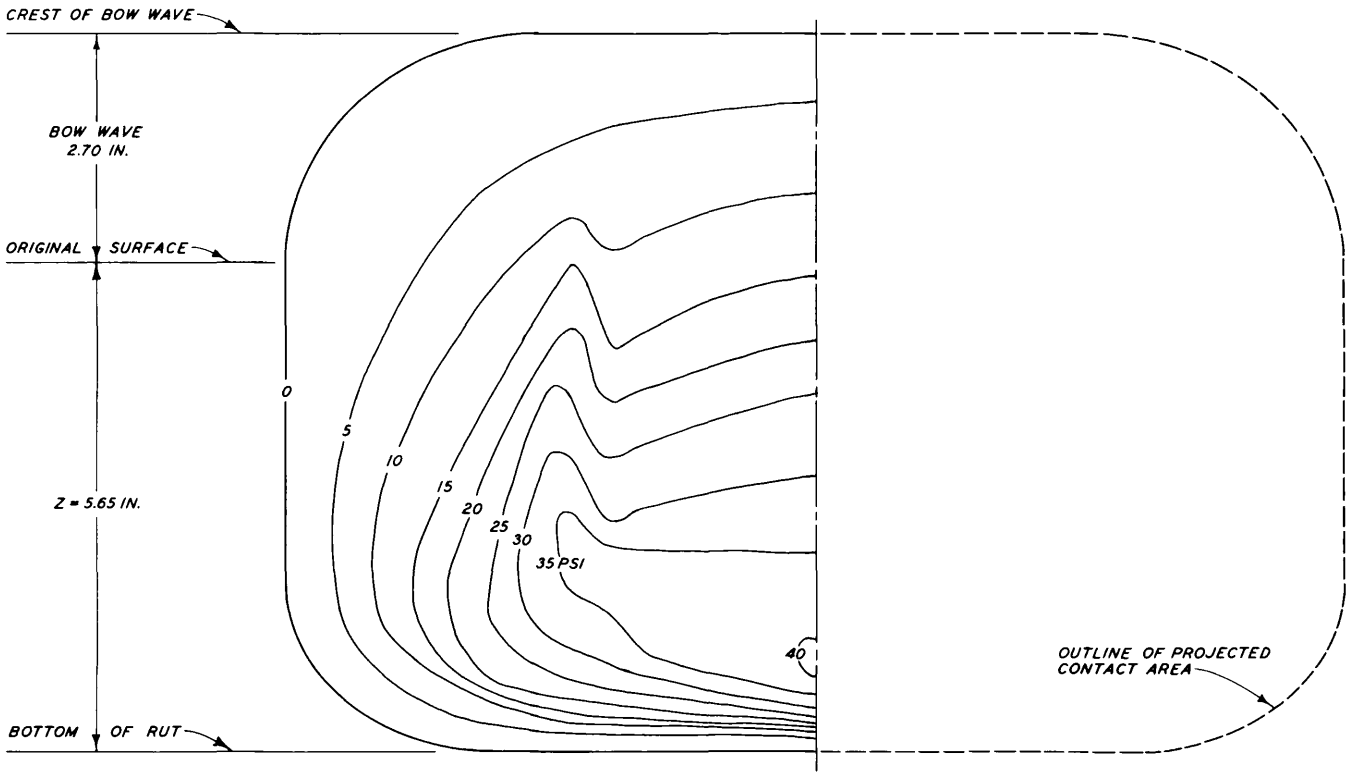

NOTE: DIRECTION OF TRAVEL IS NORMAL TO PLANE OF DRAWING.

SCALE IN INCHES

1 0 1 2 3 4

DISTRIBUTION OF NORMAL STRESSES PROJECTED ON VERTICAL PLANE

TOWED 11.00-20, 12-PR SMOOTH TIRE

3000-LB LOAD, 60-PSI INFL PRESS.

0- TO 6-IN. CONE INDEX = 27

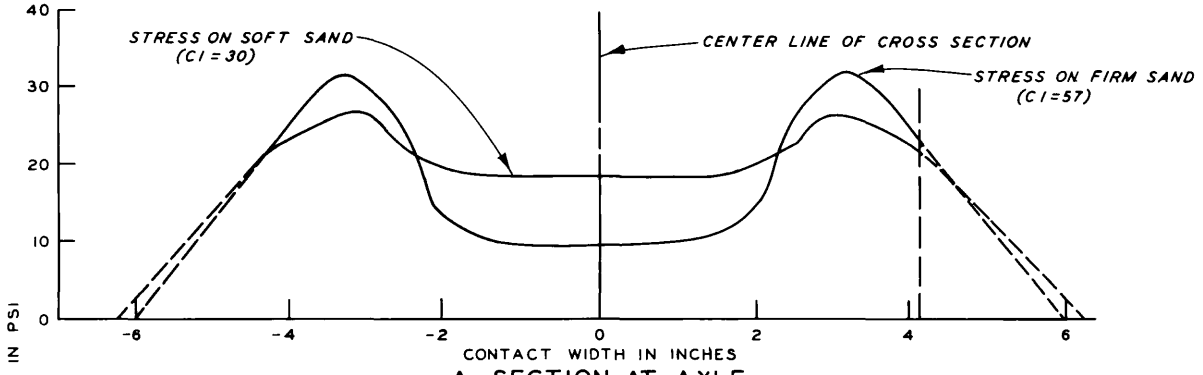

A. SECTION AT AXLE

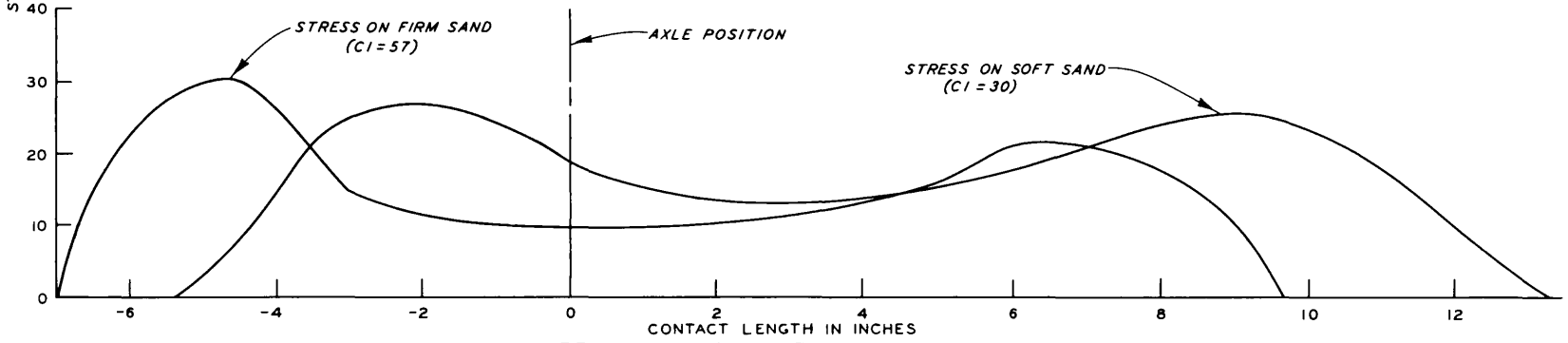

B. PROFILE ALONG CENTER LINE OF TIRE

NOTE: LENGTH AND WIDTH ARE PROJECTIONS ON A HORIZONTAL PLANE OF ACTUAL CONTACT DIMENSIONS.

DISTRIBUTION OF NORMAL STRESSES ON SAND AT TWO STRENGTHS

TOWED 11.00-20, 12-PR SMOOTH TIRE
3000-LB LOAD, 15-PSI INFL PRESS.
0- TO 6-IN. CONE INDEX = 30 AND 57

PLATE 5

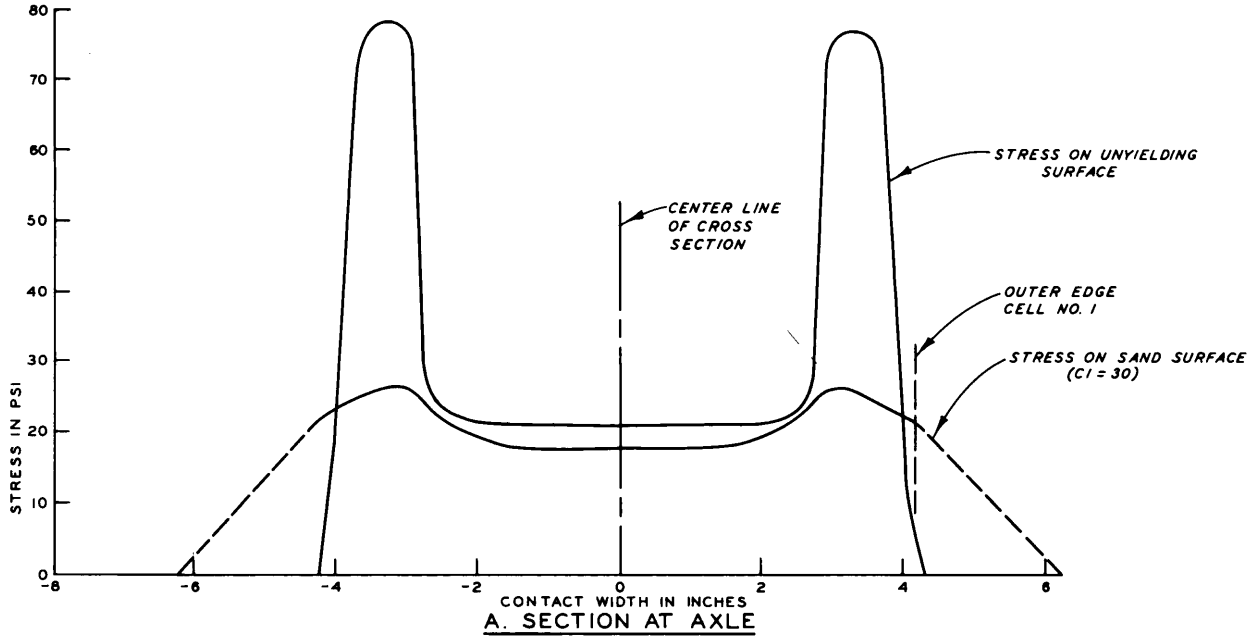

A. SECTION AT AXLE

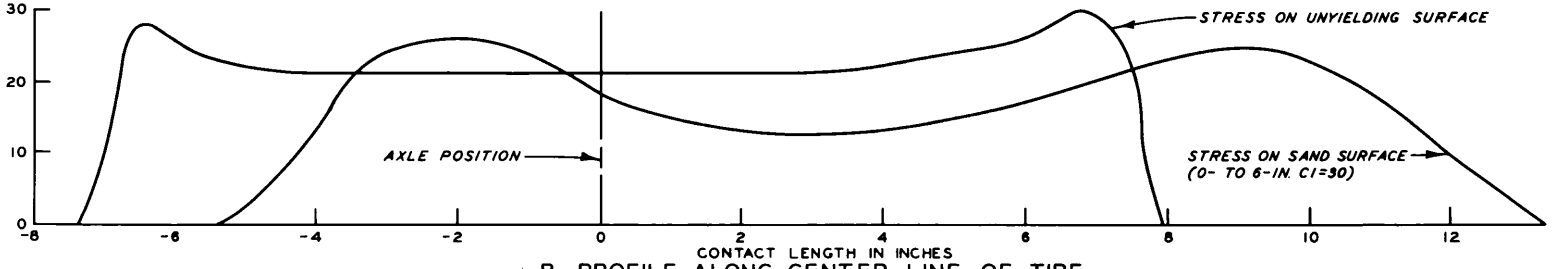

B. PROFILE ALONG CENTER LINE OF TIRE

NOTE: LENGTH AND WIDTH ON SAND ARE PROJECTIONS ON A HORIZONTAL PLANE OF ACTUAL CONTACT DIMENSIONS.

DISTRIBUTION OF NORMAL STRESSES ON TWO SURFACES

TOWED 11.00-20, 12-PR SMOOTH TIRE
3000-LB LOAD, 15-PSI INFL PRESS.
0- TO 6-IN. CONE INDEX = 30

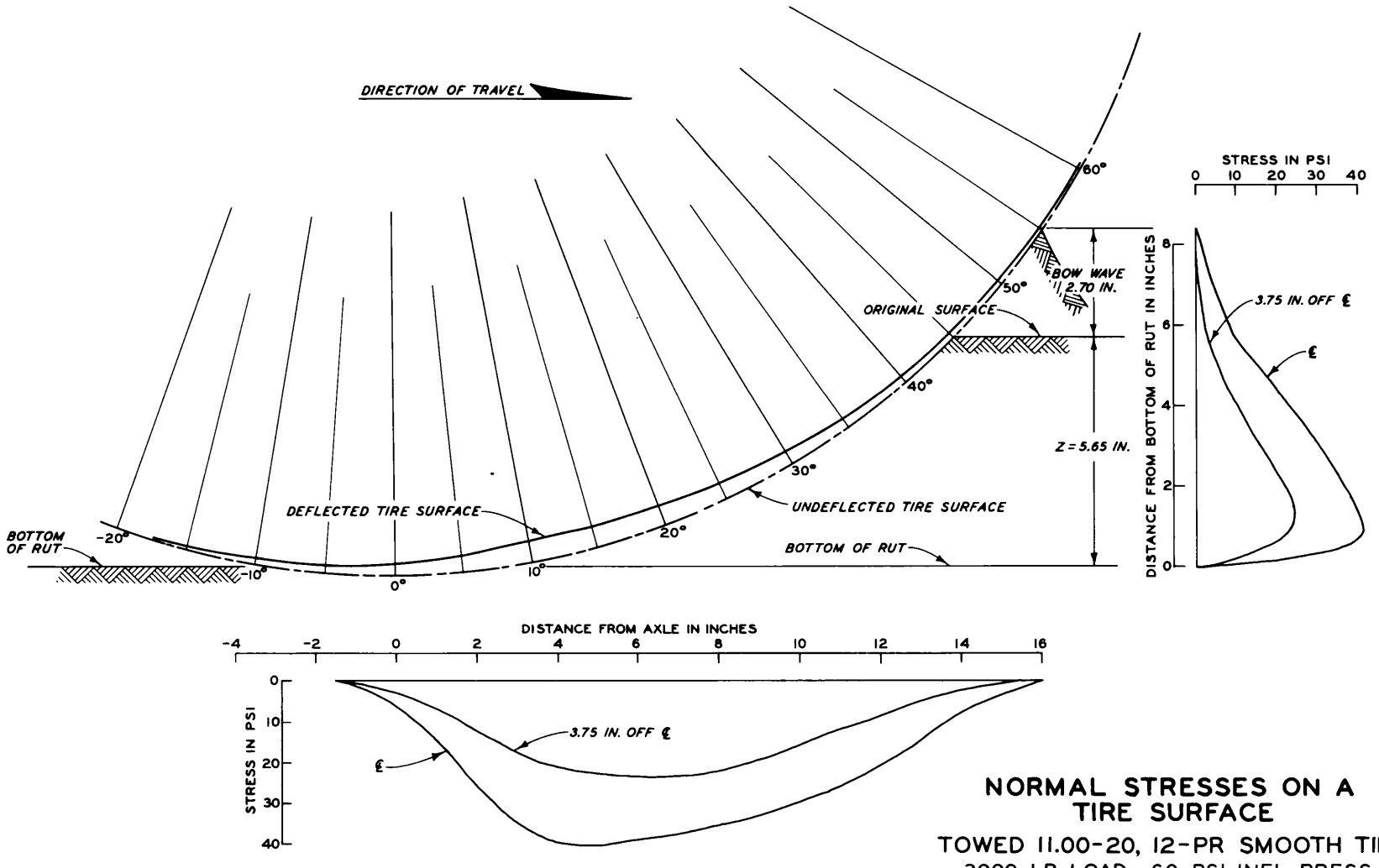

NORMAL STRESSES ON A TIRE SURFACE

TOWED 11.00-20, 12-PR SMOOTH TIRE
3000-LB LOAD, 60-PSI INFL PRESS.
MEDIUM-STRENGTH SAND
0- TO 6-IN. CONE INDEX = 27

PLATE 7

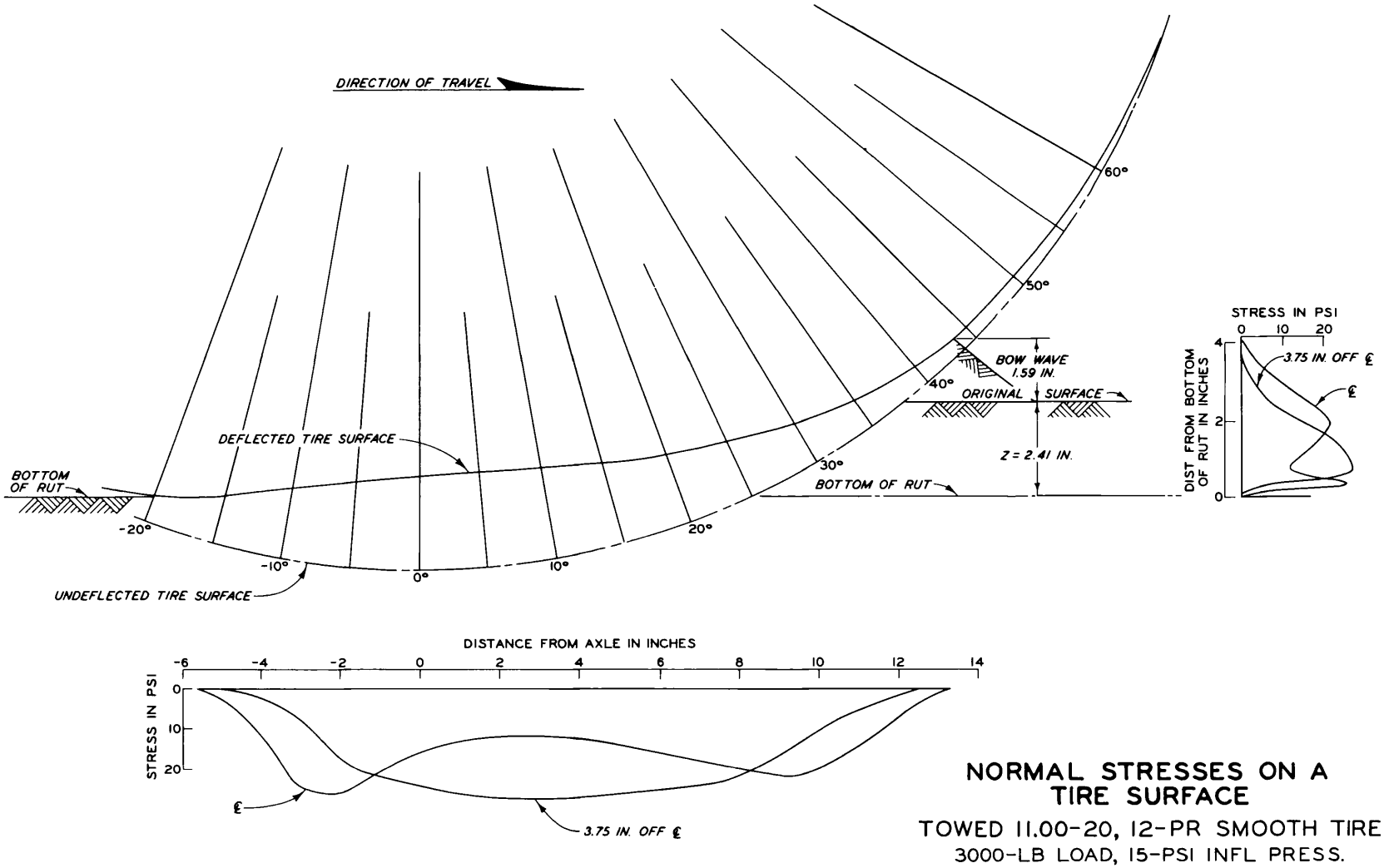

NORMAL STRESSES ON A TIRE SURFACE

TOWED 11.00-20, 12-PR SMOOTH TIRE
3000-LB LOAD, 15-PSI INFL PRESS.
MEDIUM-STRENGTH SAND
0- TO 6-IN. CONE INDEX = 30

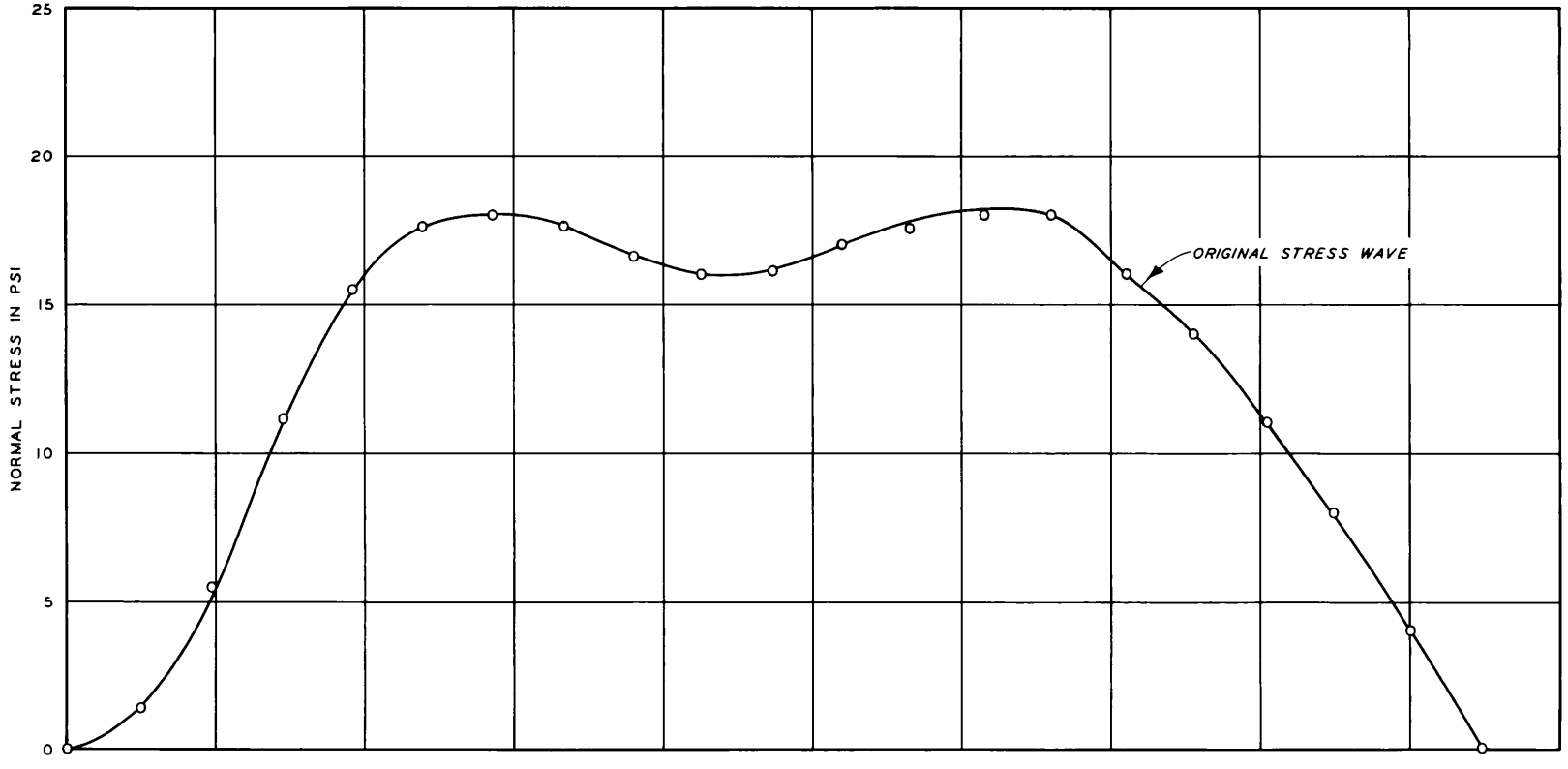

TEST CONDITIONS

TOWED 11.00-20, 12-PR SMOOTH TIRE
SOIL: MORTAR SAND (AIR DRIED)
LOAD: 3000 LB
INFLATION PRESSURE: 15 PSI

NOTE: THE POINTS REPRESENT THE SUMMATION OF THE FIRST 19 HARMONICS.

APPROXIMATION OF STRESS WAVE BY FOURIER SERIES

PLATE 9

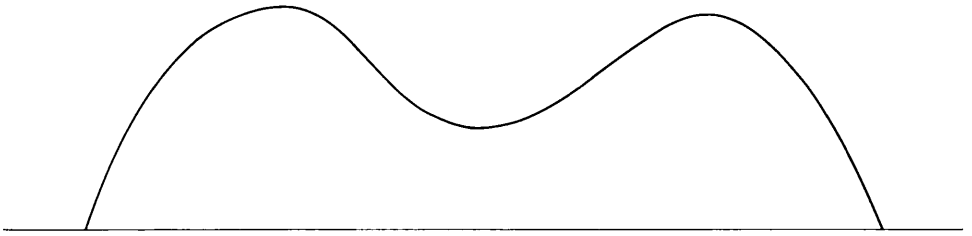

ORIGINAL STRESS WAVE

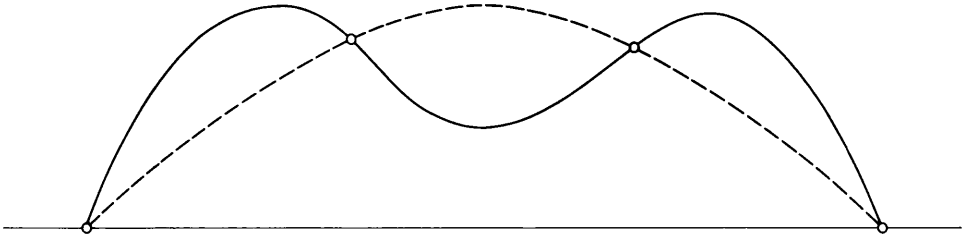

FIRST HARMONIC

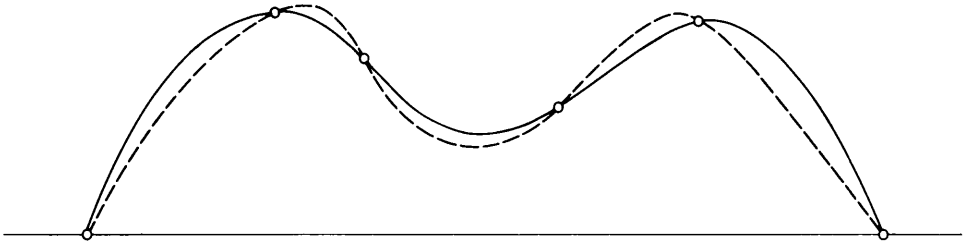

ADDITION OF FIRST AND THIRD HARMONICS

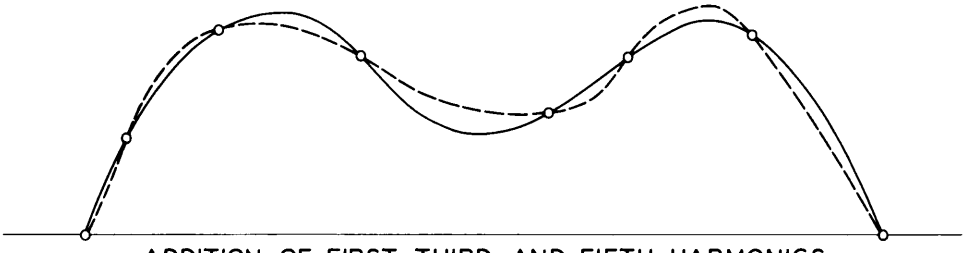

ADDITION OF FIRST, THIRD, AND FIFTH HARMONICS

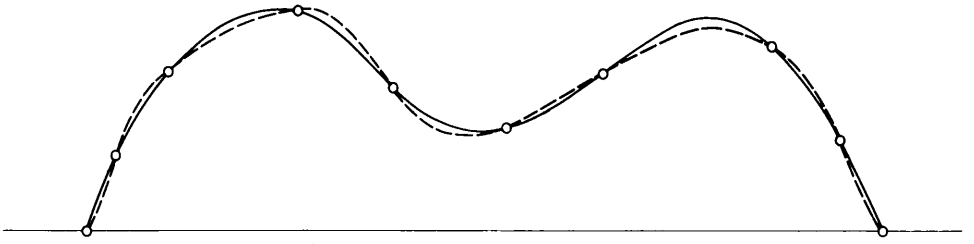

ADDITION OF FIRST, THIRD, FIFTH, AND SEVENTH HARMONICS

NOTE: EVEN HARMONICS DO NOT EXIST WHEN WAVE IS APPROXIMATED WITH AN ODD FUNCTION.

ORIGINAL STRESS WAVE AND STAGES OF APPROXIMATION BY COMBINATIONS OF HARMONICS

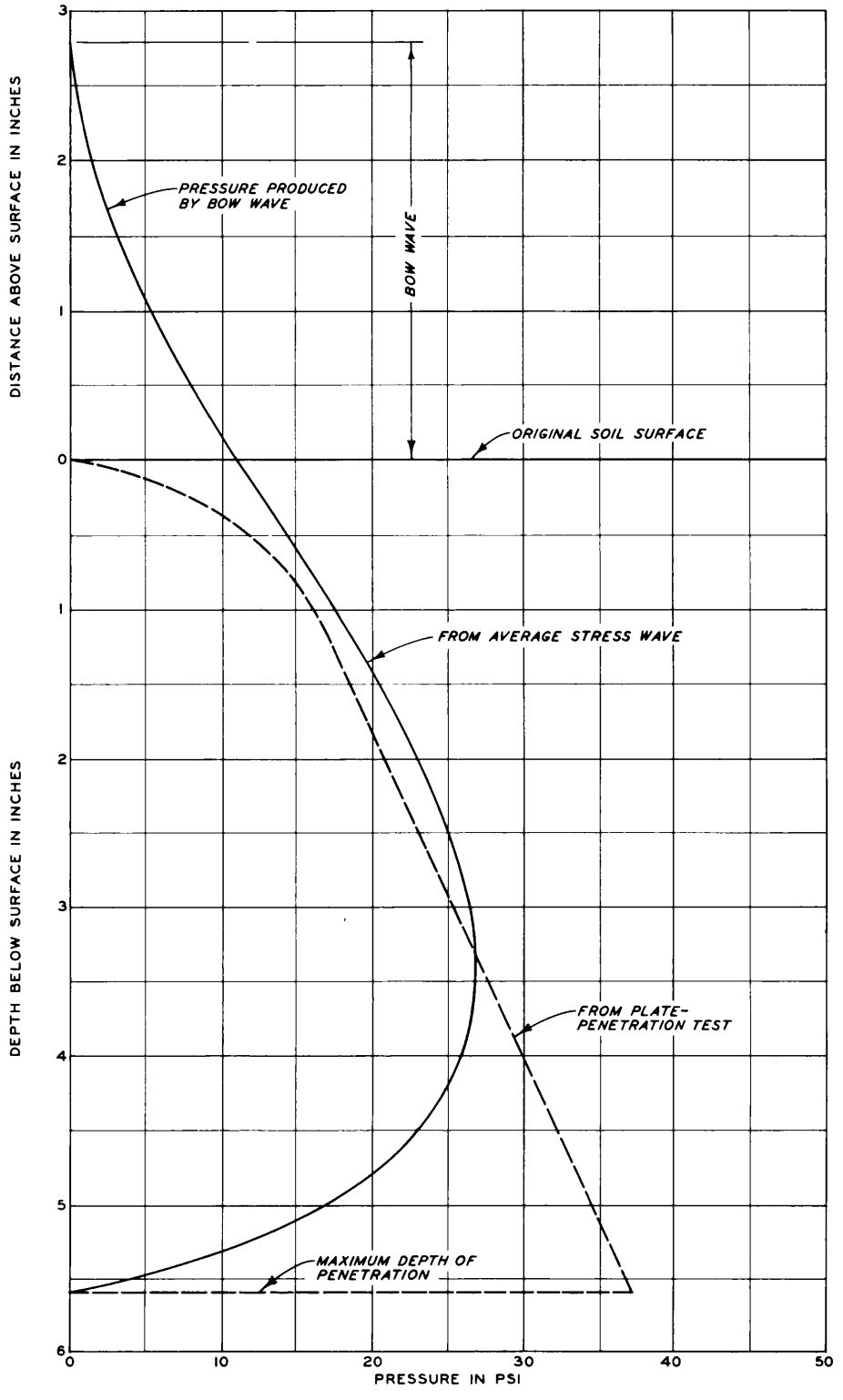

COMPARATIVE PRESSURE-SINKAGE RELATIONS IN SAND

TOWED 11.00-20, 12-PR SMOOTH TIRE AND 4.2-IN.-DIAM CIRCULAR PLATE

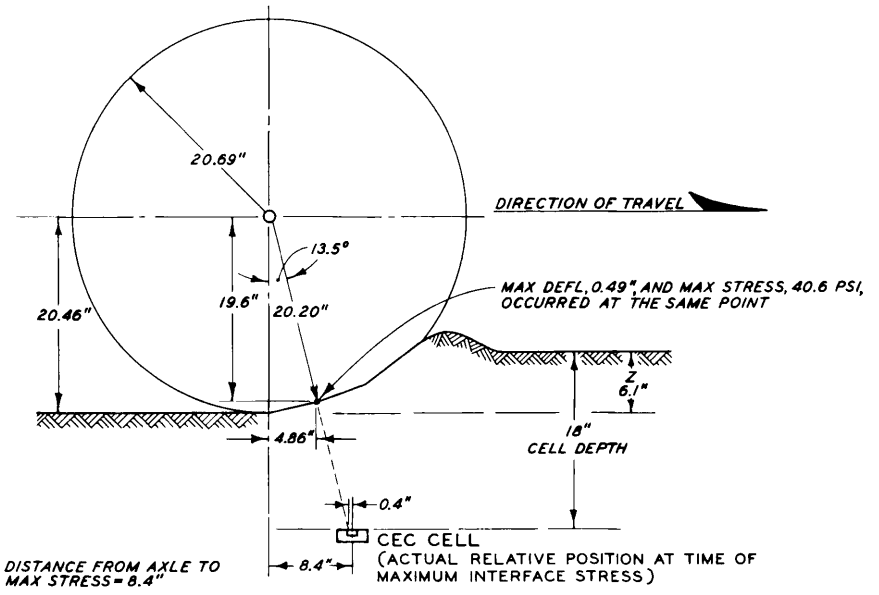

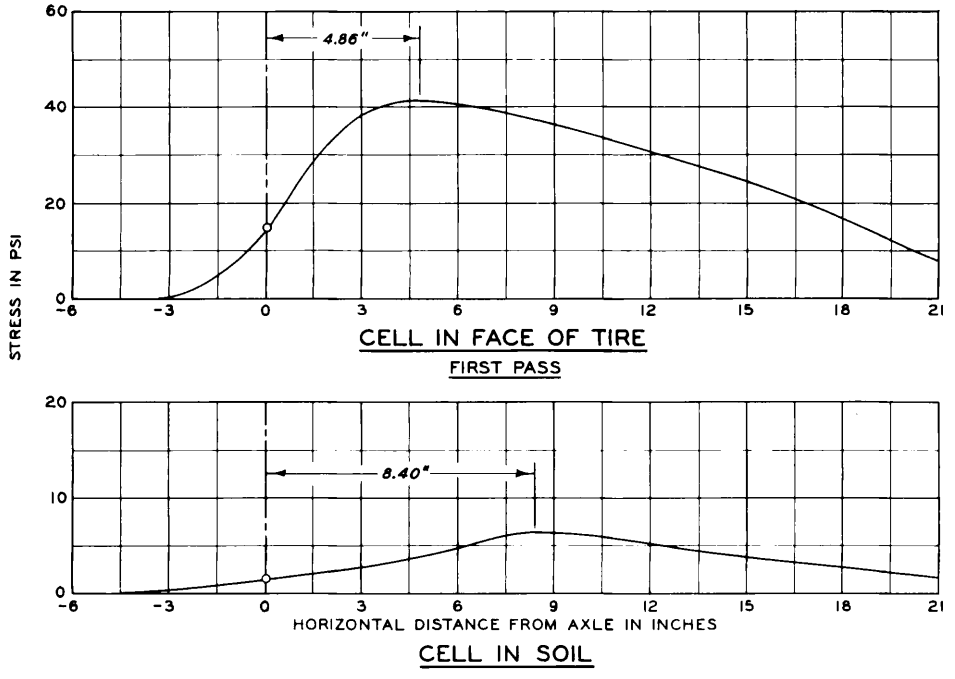

RELATIVE POSITION OF MAXIMUM STRESSES AT SURFACE AND IN SOIL MASS

TOWED 11.00-20, 12-PR SMOOTH TIRE
3000-LB WHEEL LOAD, 60-PSI INFL PRESS.
MEDIUM-STRENGTH SAND
0- TO 6-IN. CONE INDEX = 26

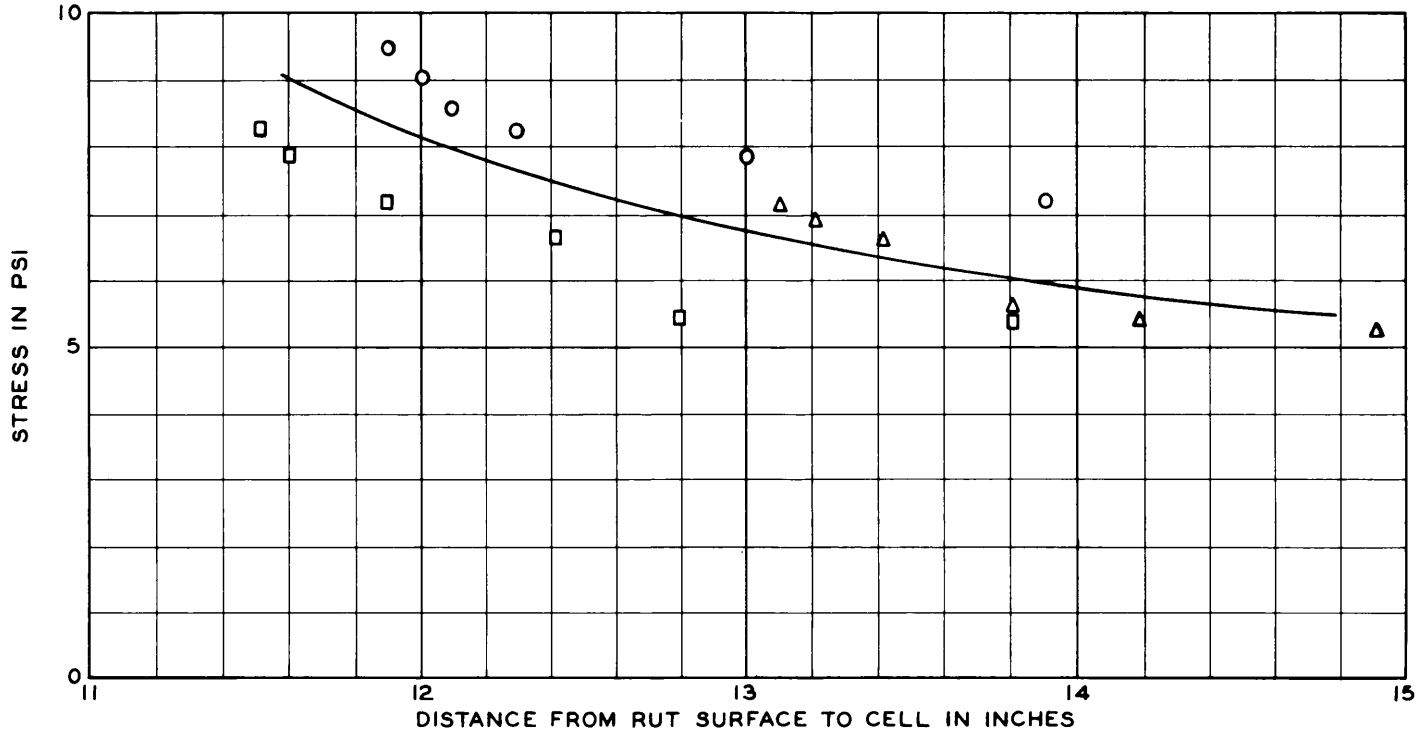

LEGEND

- ○ 0- TO 6-IN. CI = 16
- □ 0- TO 6-IN. CI = 27
- △ 0- TO 6-IN. CI = 55

NOTE: EACH POINT IS AN AVERAGE OF READINGS FROM THREE CELLS.

EFFECT OF SOIL STRENGTH ON MAXIMUM VERTICAL STRESS

TOWED 11.00-20, 12-PR SMOOTH TIRE

3000-LB WHEEL LOAD
60-PSI INFLATION PRESSURE

PLATE 13

PLATE 14

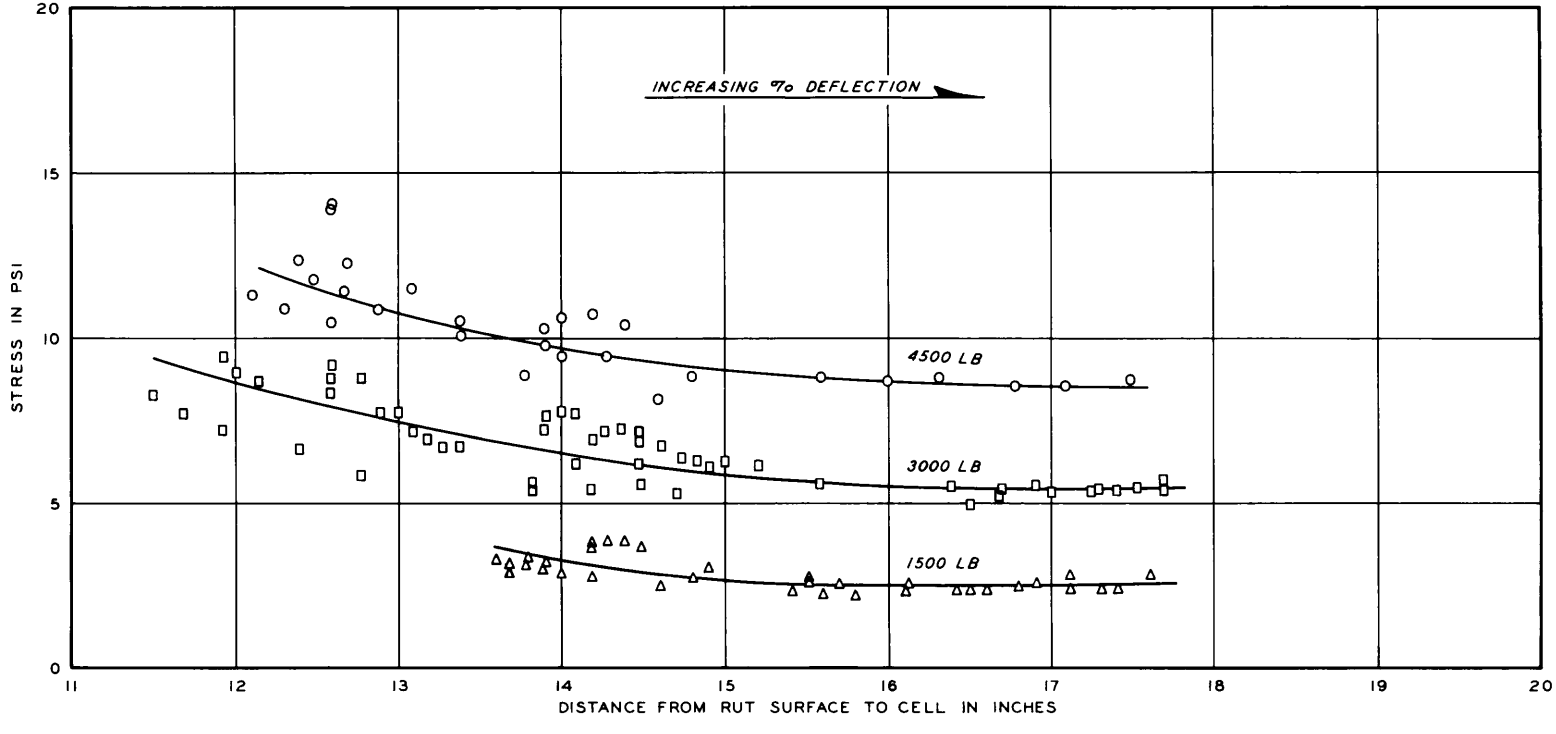

LEGEND

- ○ 4500-LB LOAD
- □ 3000-LB LOAD
- △ 1500-LB LOAD

NOTE: EACH POINT IS AN AVERAGE OF READINGS FROM THREE CELLS.

EFFECT OF LOAD ON MAXIMUM VERTICAL STRESS

TOWED 11.00-20, 12-PR SMOOTH TIRE

VARIOUS INFLATION PRESSURES AND SOIL STRENGTHS

APPENDIX A: APPLICATION OF THE FOURIER SERIES IN STRESS WAVE ANALYSIS

1. Any periodic function that satisfies the Dirichlet conditions can be represented by the sum of a number of sine waves of different frequencies.* These waves are generally referred to as harmonics. Fig. A1 shows an original stress wave and several stages of approximation by addition of harmonics. The first harmonic corresponds to the actual wave at four points. The addition of another harmonic causes the approximate wave to correspond to the actual one at two more points. Further addition of harmonics can increase the points of correspondence to any desired number; thus, an infinite series of harmonics can reproduce the curve accurately. Such an infinite series is called a Fourier series, which can be written as follows:

$$Z = f(x) = a_0 + \sum_{n=1}^{\infty} (a_n \sin nx + b_n \cos nx)$$

This equation says only that the function $f(x)$ can be expressed in terms of a constant and a series of sine and cosine functions.

2. The quantity, n, which determines the frequency of the harmonics, may take on any whole number value. To illustrate the nature of the Fourier series further, it is expanded to:

$$f(x) = a_0 + \left(a_1 \sin x + a_2 \sin 2x + a_3 \sin 3x \ldots\right) + \left(b_1 \cos x + b_2 \cos 2x + b_3 \cos 3x \ldots\right) \quad (1)$$

3. Theoretically, an infinite number of components is required to accurately represent the wave. Practically, however, only a few terms are necessary in most instances because of the relatively small effect of the terms of higher frequency.

4. The determination of the Fourier equation which specifies a

---

* The Dirichlet conditions specify that a function must be single-valued and finite, and have a finite number of discontinuities and a finite number of maxima and minima in the neighborhood of any point.

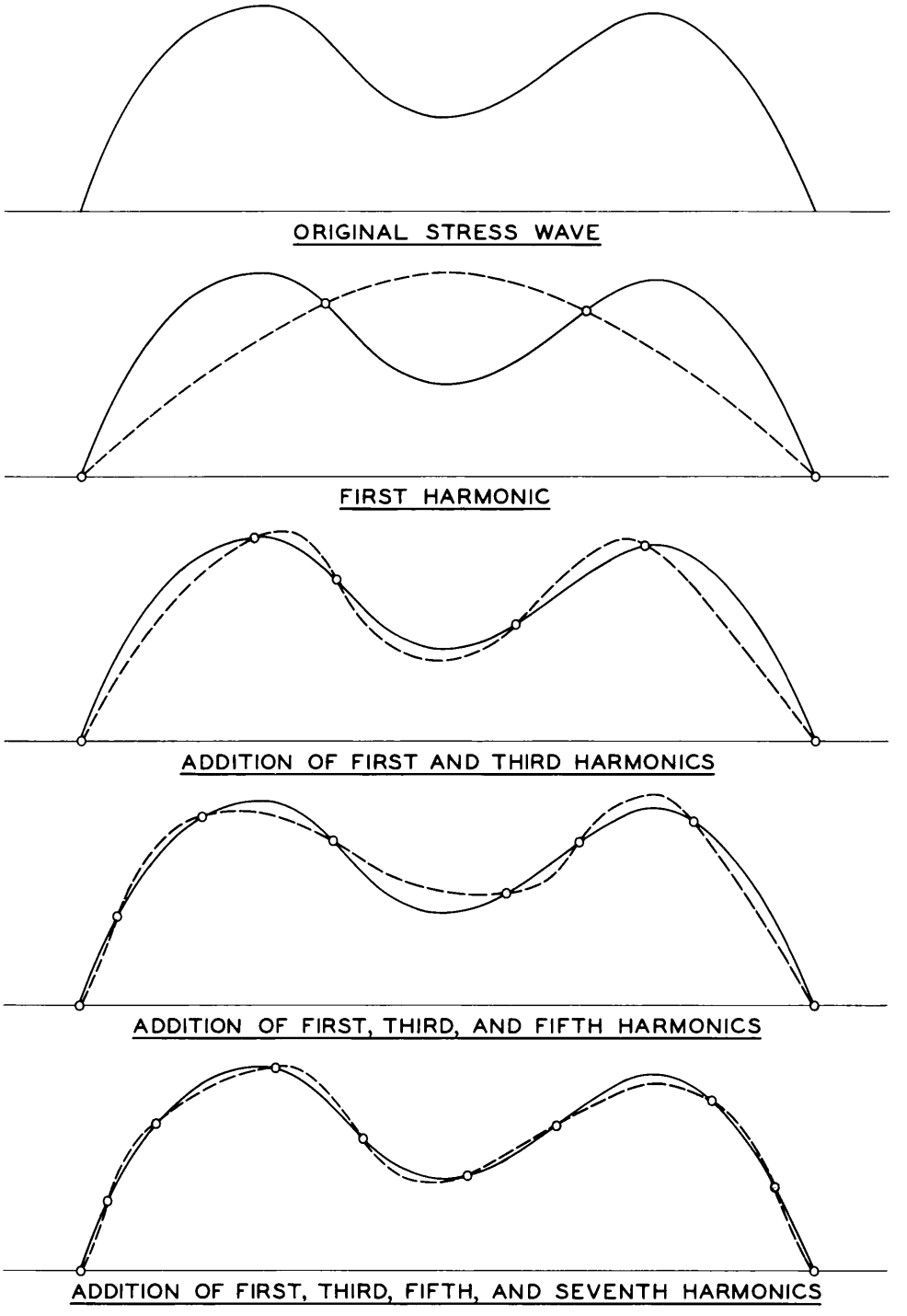

Fig. A1. Original stress wave and stages of approximation by combinations of harmonics

particular wave is called wave analysis. Wave analysis consists simply of determining the coefficients a_0 , a_1 , b_1 , etc., of equation 1. These coefficients are determined by some operation on the equation that will eliminate all terms except the desired quantity. Then the desired coefficient can be evaluated. Thus, to determine a_0 , it is necessary simply to multiply equation 1 by dx and integrate between 0 and 2π as shown below:

$$\int_0^{2\pi} f(x)\,dx = \int_0^{2\pi} a_0\,dx + \int_0^{2\pi} a_1 \sin x\,dx + \int_0^{2\pi} a_2 \sin 2x\,dx + \ldots$$

$$+ \int_0^{2\pi} b_1 \cos x\,dx + \int_0^{2\pi} b_2 \cos 2x\,dx + \int_0^{2\pi} b_3 \cos 3x\,dx + \ldots$$

or

$$\int_0^{2\pi} f(x)\,dx = a_0 \int_0^{2\pi} dx = a_0 2\pi$$

$$\therefore a_0 = \frac{1}{2\pi} \int_0^{2\pi} f(x)\,dx \qquad (2)$$

This equation represents the average height of the curve over a complete period. To evaluate the remaining coefficients for a particular problem, the following convenient mathematical relations are used:

(a) $$\int_0^{2\pi} \sin mx \sin nx\,dx = \begin{cases} 0 \text{ if } m \neq n \\ \pi \text{ if } m = n \end{cases}$$

(b) $$\int_0^{2\pi} \cos mx \sin nx\,dx = 0 \text{ if } m \neq n$$

(c) $$\int_0^{2\pi} \cos x \sin x\,dx = 0$$

(d) $$\int_0^{2\pi} \sin^2 x\,dx = \pi$$

To find a_1 for instance, equation 1 can be multiplied by $\sin x\,dx$ and integrated from 0 to 2π. Thus:

$$\int_0^{2\pi} f(x) \sin x\,dx = a_0 \int_0^{2\pi} \sin x\,dx + a_1 \int_0^{2\pi} \sin^2 x\,dx + \ldots$$

$$+ b_1 \int_0^{2\pi} \cos x \sin x\,dx + b_2 \int_0^{2\pi} \cos 2x \sin x\,dx + \ldots$$

It is obvious that $a_0 \int_0^{2\pi} \sin x\,dx$ is zero since it represents the area under a sine wave for a complete cycle. Hence, from the given relation,

$$\int_0^{2\pi} f(x) \sin x\,dx = a_1 \pi$$

or

$$a_1 = \frac{1}{\pi} \int_0^{2\pi} f(x) \sin x\,dx \tag{3}$$

This process is repeated, multiplying equation 1 by $\sin 2x$, $\sin 3x$, etc. This yields the general equation:

$$a_n = \frac{1}{\pi} \int_0^{2\pi} f(x) \sin nx\,dx \tag{4}$$

To evaluate the coefficient of the cosine term b_1, equation 1 is multiplied by $\cos x\,dx$ and integrated from 0 to 2π. If the preceding relations are used, the results are:

$$\int_0^{2\pi} f(x) \cos x\,dx = b_1 \pi$$

or

$$b_1 = \frac{1}{\pi} \int_0^{2\pi} f(x) \cos x\,dx \tag{5}$$

Other operations yield the general equation:

$$b_n = \frac{1}{\pi} \int_0^{2\pi} f(x) \cos nx \, dx \qquad (6)$$

5. If the equation of Z in terms of x is known in some mathematical form, the wave can be analyzed analytically. This method cannot be employed if the function of x is not known analytically.

6. The equation of Z in terms of x is usually unknown. It is under these conditions that a step-by-step (graphical method) procedure is employed as follows.* Suppose the wave in fig. A2 is to be analyzed. The term a_0, which represents the average height of the curve over a complete period (2π radians), is found by dividing the area under the curve by the base. If the areas of the positive and negative loops are the same, a_0 is zero.

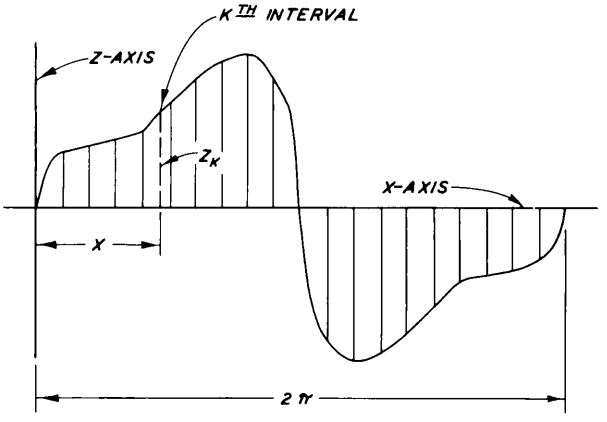

Fig. A2. Preparation of a wave for analysis by the graphical method

7. For graphical analysis, equation 3 can be expressed mathematically as:

$$a_1 = \frac{1}{\pi} \sum_0^{2\pi} f(x) \sin x \, \Delta x \qquad (7)$$

Let 2π radians in fig. A2 be divided into m equal parts. Then $\Delta x = \frac{2\pi}{m}$ and x, the distance to the midpoint of the Kth interval, is

$$K \frac{2\pi}{m} - \frac{1}{2}\left(\frac{2\pi}{m}\right) \text{ or } \left(K - \frac{1}{2}\right)\frac{2\pi}{m}$$

The equation can now be written as:

---

* The synopsis in paragraphs 6-8 on the procedures of the graphical method was paraphrased from the text, "Alternating Current Circuits," pp 234-235, written by Russel M. Kerchner and George F. Corcoran.

$$a_1 = \frac{1}{\pi} \sum_{0}^{m} \left[Z_k \sin \left(K - \frac{1}{2} \right) \frac{2\pi}{m} \right] \frac{2\pi}{m}$$

$$= \frac{2\pi}{m} \frac{1}{\pi} \sum_{0}^{m} Z_k \sin \left[\left(K - \frac{1}{2} \right) \frac{2\pi}{m} \right]$$

$$= \frac{2}{m} \sum_{0}^{m} Z_k \sin \left[\left(K - \frac{1}{2} \right) \frac{2\pi}{m} \right] \tag{8}$$

Similarly

$$b_1 = \frac{2}{m} \sum_{0}^{m} Z_k \cos \left[\left(K - \frac{1}{2} \right) \frac{2\pi}{m} \right] \tag{9}$$

8. Multiplying and dividing equation 7 by 2 yields:

$$a_1 = 2 \left[\frac{1}{2\pi} \sum_{0}^{2\pi} f(x) \sin x \, \Delta x \right]$$

This indicates that a_1 is twice the average ordinate of the new curve which would be obtained by plotting corresponding ordinates of the original curve multiplied by the sine of the angle to the ordinate in question. Similar interpretations can be drawn regarding the other coefficients of the Fourier series.

9. Fig. A3a shows a wave representing the average stresses across the face of a tire, while fig. A3b illustrates the manner in which this average wave is prepared for wave analysis. The stress wave is represented in the form shown in fig. A3b in order to simplify the analysis. The wave is represented over a distance of π radians as its length. It is then reproduced asymmetrically below the axis, so that the entire distance is 2π radians. This, in essence, produces an odd periodic function. The positive and negative loops have the same areas; hence the constant term a_0 is zero. When $f(-x) = -f(x)$, the function is called an odd function and no cosine terms exist.* Table A1 shows the computations involved

* R. V. Churchill, Fourier Series and Boundary Value Problems, Chapter IV, pp 57 and 58.

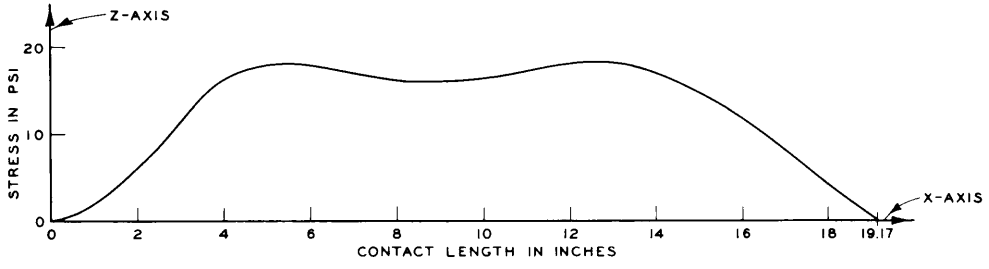

a. Average stress wave

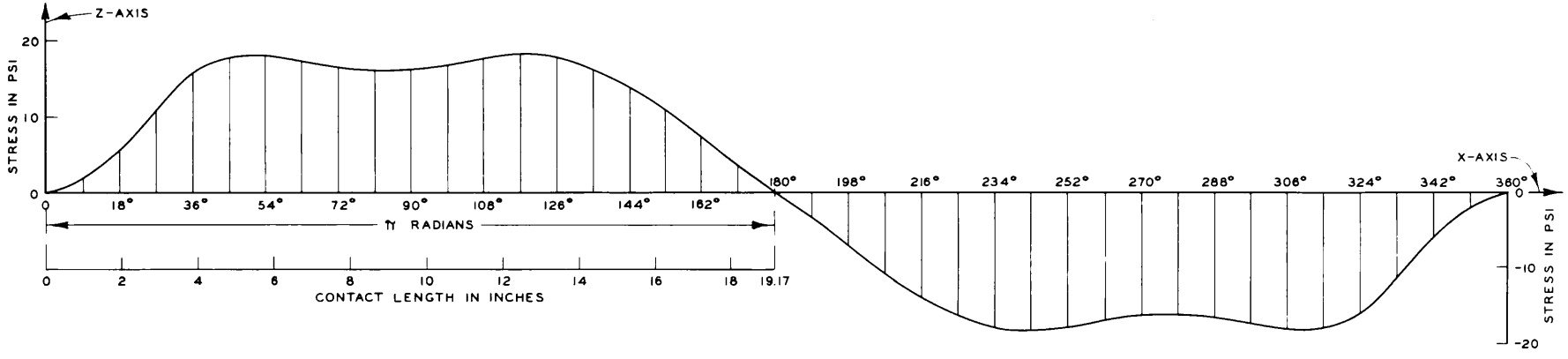

b. Preparation of average stress wave for Fourier analysis (asymmetrical)

Fig. A3. Average stress wave, and manner in which it is prepared for Fourier analysis

in obtaining the Fourier coefficients and reveals why the cosine coefficients become zero for an odd function.

10. By preparing the wave in this manner, the series representing the wave is reduced to:

$$f(x) = \sum_{n=1}^{\infty} a_n \sin nx \qquad (10)$$

The above form is generally called a sine series. A computer program which employs the graphical method for determining coefficients has been prepared. This is an expedient method of determining coefficients for any particular wave to be analyzed. Table A2 shows the values of the coefficients obtained by the computer for the data representing the wave in fig. A3b. It should be noted that the summation of 19 harmonics was used to approximate the wave. The resulting equation is therefore written as follows:

$$Z = 19.8 \sin x + 2.7 \sin 3x - 0.1 \sin 4x - 1.3 \sin 5x - 0.9 \sin 6x$$
$$- 0.4 \sin 7x - 0.4 \sin 8x - 0.2 \sin 9x - 0.2 \sin 10x$$
$$- 0.1 \sin 11x + 0.1 \sin 12x - 0.1 \sin 17x + 0.1 \sin 18x$$

It will be noted that the coefficients of the terms, $n = 2$ and $n = 19$, were zero.

11. This equation represents the periodic wave for all values of x. However, the distance which represents the original stress wave is defined by the value of x from 0 to π.

12. Information concerning the load on the wheel, the force required to tow the tire, and the location and magnitude of the resulting external forces (soil reaction) acting on the wheel can be obtained from this Fourier equation. The first step in this analysis is to determine the area under the original stress wave. This is accomplished by integrating each term of the equation over the interval 0 to π and summing the results. An example of the computations involved is given below.

$$A = 19.8 \int_0^{\pi} \sin x \, dx + 2.7 \int_0^{\pi} \sin 3x \, dx - 0.1 \int_0^{\pi} \sin 4x \, dx \ldots$$

$$= 19.8 \left[-\cos\ x \right]_0^{\pi} + \frac{2.7}{3} \left[-\cos\ 3x \right]_0^{\pi} - \frac{0.1}{4} \left[-\cos\ 4x \right]_0^{\pi} \ldots$$

$$= 19.8\ [2] + \frac{2.7}{3}\ [2] - \frac{0.1}{4}\ [-0]$$

The terms containing even multiples of x (i.e. terms in which n is an even integer) obviously become zero when the limits are substituted, and the terms containing odd multiples of x become a product of the integer 2 and their respective coefficient divided by the corresponding multiple of x. Hence, the computations involved are reduced to the following:

$$A = 2 \left(19.8 + \frac{2.7}{3} - \frac{1.3}{5} - \frac{0.4}{7} - \frac{0.2}{9} - \frac{0.1}{11} - \frac{0.1}{17} \right)$$

$$A = 2 \left(20.346 \right) = 40.692$$

13. The resulting numerical value of 40.692 represents pounds per square inch per π radians. The measured length of the stress wave is 19.17 in. Having represented the length over a distance of π radians, a conversion factor $\left(\frac{19.17}{\pi} \right)$ is utilized to convert radians to inches. In order to obtain the area under the curve in the desired system, the following computation is necessary

$$40.692 \times \frac{19.17}{3.1416} = 248.30 \text{ lb/in.}$$

The distance, 19.17 in., was determined by the vertical projection of the tire's contact length on a horizontal plane (see fig. A4). Therefore, multiplying the area under the curve by the effective width (which for this test was 12.5 in.) results in a volumetric value (lb/in. $\times$ in.) which is approximately equal to the vertical load acting on the wheel.

14. The computation gives the following results:

248.30 lb per in. $\times$ 12.5 in. = 3104 lb = computed vertical load

The next step in this analysis is to determine the location of the vertical force (F_z). The logical approach to this problem is to locate

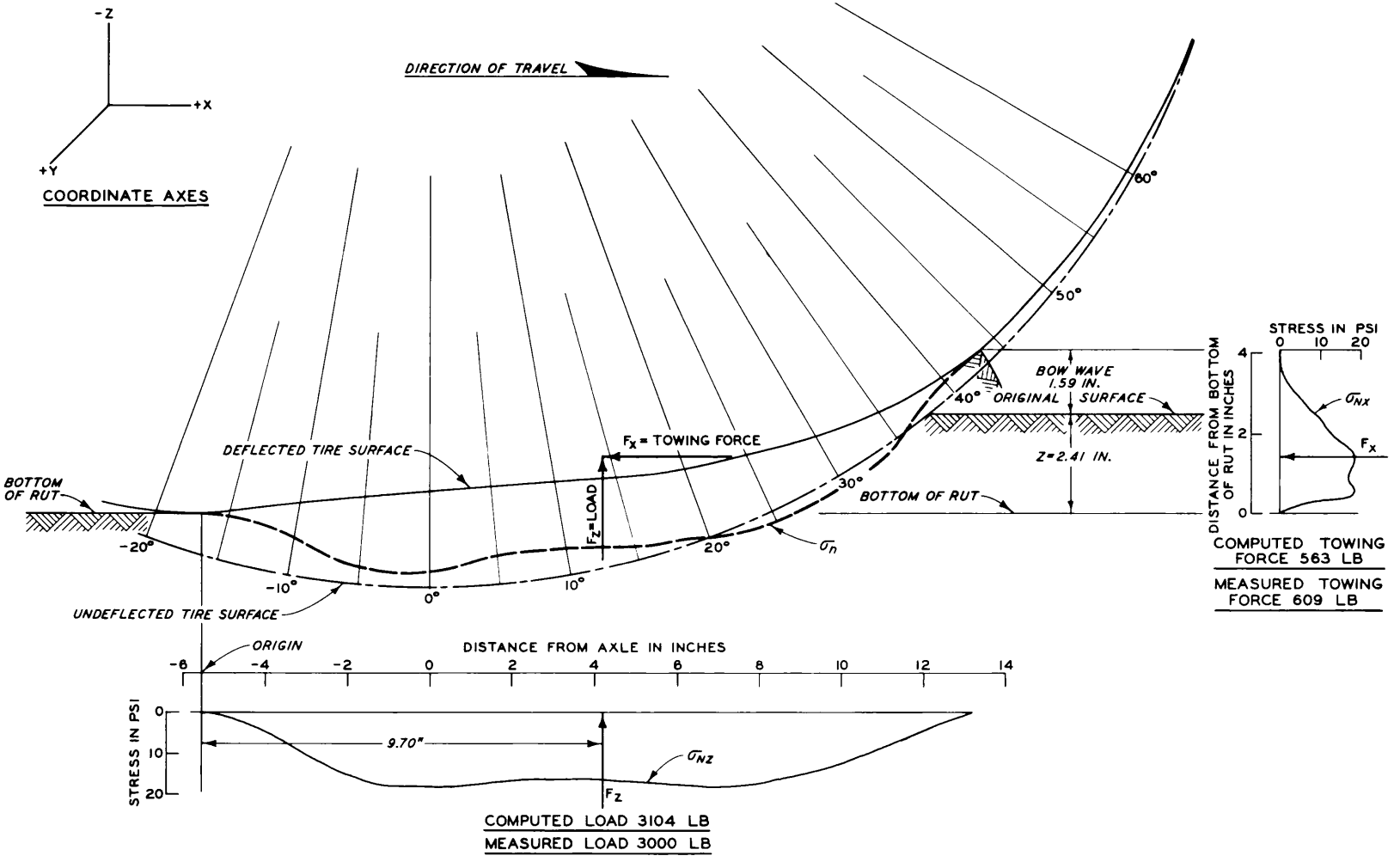

Fig. A4. Normal stresses on a tire surface. Towed 11.00-20, 12-PR smooth tire; 3000-lb load, 15-psi inflation pressure; medium-strength sand, 0- to 6-in. cone index = 30

the centroid of the volume under the curve. The centroid is determined by the coordinates $\bar{x}$, $\bar{y}$, and $\bar{z}$. The use of average stress values provides an axis of symmetry (the x-axis) which bisects the effective contact width. Therefore, the centroid will lie on that axis. This eliminates the necessity of computing $\bar{y}$. The stress distribution pattern can now be represented as a two-dimensional curve in the $x - z$ plane. The computation of $\bar{z}$ is not necessary for this analysis because the location of the resultant stress is dependent only on the values $\bar{y}$ and $\bar{x}$. Hence, the only computation to be made in locating this resultant is to determine the value $\bar{x}$. The relation between $\bar{x}$ and the moments of area is given by the equation:

$$\bar{x} = \frac{M_z}{A}$$

where

M_z = moments of area about z-axis

A = area under the stress curve

15. To calculate $\bar{x}$, the following mathematical equation is used:

$$M_z = \int_0^{\pi} xz \, dx$$

Using this relation and substituting the Fourier expression for z (page 70), the following equation is obtained:

$$M_z = \int_0^{\pi} x \, (19.8 \sin x + 2.7 \sin 3x + \ldots) \, dx$$

or

$$M_z = 19.8 \int_0^{\pi} x \sin x \, dx + \frac{2.7}{3} \int_0^{\pi} x \sin 3x \, 3dx + \ldots$$

The following step-by-step computations reveal the simplicity of this operation. Taking the first term, we have:

(a) $$19.8 \int_0^{\pi} x \sin x \, dx$$

Integration by parts yields:

(b) $$19.8 \left[-x \cos x + \sin x \right]_0^{\pi}$$

Substituting the limits yields:

(c) $$19.8 \left[\pi \right]$$

Now, taking the third term of the original equation which contains an even multiple of x :

(a) $$\frac{-0.1}{4} \int_0^{\pi} x \sin 4x \, 4dx$$

Integration by parts yields:

(b) $$\frac{-0.1}{4} \left[-x \cos 4x + \frac{\sin 4x}{4} \right]_0^{\pi}$$

Substituting the limits yields:

(c) $$\frac{-0.1}{4} \left[-\pi \right]$$

This occurrence is valid throughout for every term; that is, terms containing odd multiples of x become a product of π and the respective coefficient divided by the corresponding multiple of x . Terms containing even multiples of x become a product of $(-\pi)$ and the ratio of the coefficient and its respective multiple. Therefore, the computations result in the following equation:

$$M_z = 19.8 (\pi) + \frac{2.7}{3} (\pi) - \frac{0.1}{4} (-\pi) - \frac{1.3}{5} (\pi) + \ldots$$

which, when factored, becomes:

$$M_z = \pi \left(19.8 + \frac{2.7}{3} + \frac{0.1}{4} - \frac{1.3}{5} + \ldots\right)$$

Summation of the terms yields:

$$M_z = 20.58\pi$$

By use of the conversion ratio:

$$M_z = \frac{19.17}{3.1416}(20.58)\pi = 125.58\pi \text{ lb/in.}$$

Finally, substitution in the equation gives:

$$\bar{x} = \frac{M_z}{A} = \frac{125.58\pi \text{ lb/in.}}{248.30 \text{ lb/in.}} = 0.506\pi$$

Since $\pi = 3.1416$ radians = 19.17 in., it follows that:

$$\bar{x} = 0.506\ (19.17) = 9.7 \text{ in.}$$

16. The resultant vertical force (F_z) is therefore located along the x-axis at a position 9.7 in. from the origin.

17. The same analysis is applied to the horizontal stresses (normal stress projected in a vertical plane) to obtain the horizontal force (F_x). Fig. A4 reveals the results obtained from this analysis.

18. Although this method may appear somewhat complex, the mechanics involved are relatively simple. The electronic computer program written specifically for this analysis provides an expedient method enabling a more comprehensive study of the external forces acting on a towed pneumatic tire.

Table A1

First Harmonic

Ordinate No.	Measured Ordinate z	x deg	Sin x	Products (z sin x) Plus Value	Products (z sin x) Minus Value	Cos x	Products (z cos x) Plus Value	Products (z cos x) Minus Value
1	1.5	9	0.15643	0.23	0	0.98769	1.48	
2	5.5	18	0.30902	1.70		0.95106	5.23	
3	11.0	27	0.45399	4.99		0.89101	9.80	
4	15.5	36	0.58779	9.11		0.80902	12.54	
5	17.6	45	0.70711	12.44		0.70711	12,44	
6	18.0	54	0.80902	14.56		0.58779	10.58	
7	17.6	63	0.89101	15.68		0.45399	7.99	
8	16.5	72	0.95106	15.69		0.30902	5.10	
9	16.0	81	0.98769	15.80		0.15643	2.50	
10	16.0	90	1.00000	16.00		0.00000	0.00	
11	17.0	99	0.98769	16.79		-0.15643		2.66
12	17.5	108	0.95106	16.64		-0.30902		5.41
13	18.0	117	0.89101	16.04		-0.45399		8.17
14	18.0	126	0.80902	14.56		-0.58779		10.58
15	16.0	135	0.70711	11.31		-0.70711		11.31
16	14.0	144	0.58779	8.23		-0.80902		11.33
17	11.0	153	0.45399	4.99		-0.89101		9.80
18	8.0	162	0.30902	2.47		-0.95106		7.61
19	4.0	171	0.15643	0.63		-0.98769		3.95
20	0.0	180	0.00000	0.00		-1.00000		0.00
21	-4.0	189	-0.15643	0.63		-0.98769	3.95	
22	-8.0	198	-0.30902	2.47		-0.95106	7.61	
23	-11.0	207	-0.45399	4.99		-0.89101	9.80	
24	-14.0	216	-0.58779	8.23		-0.80902	11.33	
25	-16.0	225	-0.70711	11.31		-0.70711	11.31	
26	-18.0	234	-0.80902	14.56		-0.58779	10.58	
27	-18.0	243	-0.89101	16.04		-0.45399	8.17	
28	-17.5	252	-0.95106	16.64		-0.30902	5.41	
29	-17.0	261	-0.98769	16.79		-0.15643	2.66	
30	-16.0	270	-1.00000	16.00		0.00000	0.00	
31	-16.0	279	-0.98769	15.80		0.15643		2.50
32	-16.5	288	-0.95106	15.69		0.30902		5.10
33	-17.6	297	-0.89101	15.68		0.45399		7.99
34	-18.0	306	-0.80902	14.56		0.58779		10.58
35	-17.6	315	-0.70711	12.44		0.70711		12.44
36	-15.5	324	-0.58779	9.11		0.80902		12.54
37	-11.0	333	-0.45399	4.99		0.89101		9.80
38	-5.5	342	-0.30902	1.70		0.95106		5.23
39	-1.5	351	-0.15643	0.23		0.98769		1.48
40	0.0	360	0.00000	0.00		1.00000		0.00
				395.72	0		138.48	-138.48

Sum of products 395.72 0

$$a_1 = \frac{395.72}{40} \times 2 = 19.8 \qquad b_1 = 0$$

Table A2

Values Representing the Fourier Coefficients

b_0	0		
b_1	0	a_1	19.8
b_2	0	a_2	0
b_3	0	a_3	2.7
b_4	0	a_4	-0.1
b_5	0	a_5	-1.3
b_6	0	a_6	-0.9
b_7	0	a_7	-0.4
b_8	0	a_8	-0.4
b_9	0	a_9	-0.2
b_{10}	0	a_{10}	-0.2
b_{11}	0	a_{11}	-0.1
b_{12}	0	a_{12}	0.1
b_{13}	0	a_{13}	0
b_{14}	0	a_{14}	0
b_{15}	0	a_{15}	0
b_{16}	0	a_{16}	0
b_{17}	0	a_{17}	-0.1
b_{18}	0	a_{18}	0.1
b_{19}	0	a_{19}	0

DISTRIBUTION LIST

Address	No. of Copies
Commanding General, U. S. Army Materiel Command ATTN: AMCRD-RV-E Washington, D. C.	2
Commanding Officer, USACRREL ATTN: Library, P. O. Box 282 Hanover, N. H.	1
President U. S. Army Armor Board Fort Knox, Ky.	1
Commanding General, U. S. Army Weapons Command ATTN: AMSWE-RDR Rock Island, Ill.	1
Commanding General, U. S. Army Tank-Automotive Center ATTN: SMOTA-RCL Warren, Mich.	1
Commanding Officer, Rock Island Arsenal ATTN: SWERI-RDD-TS Rock Island, Ill.	1
Commanding Officer, Yuma Proving Ground ATTN: STEYT-TGM Yuma, Ariz.	1
President U. S. Army Infantry Board Fort Benning, Ga.	1
Technical Library, Branch No. 4 U. S. Army Limited War Laboratory, Building 359 Aberdeen Proving Ground, Md.	1
British Liaison Officer (thru AMC, ATTN: AMCIS-SI)	4
Canadian Liaison Officer (thru AMC, ATTN: AMCIS-SI)	3
Automotive Engineering Laboratory ATTN: STEAP-DP-LU Aberdeen Proving Ground, Md.	1

Address	No. of Copies
President U. S Army Artillery Board Fort Sill, Okla.	1
Commander, U. S. Army Picatinny Arsenal, ATTN: SMUPA-VC1, Mr. D. Sen Dover, N. J.	1
Commanding Officer, Hqs, U. S. Army Materiel Command Field Office Fort Benning, Ga.	2
Commanding Officer, USA Engineer Research and Development Laboratories ATTN: Technical Document Center Fort Belvoir, Va.	2
Commanding Officer, USA Electronics Research and Development Activity, Ariz. ATTN: SELHU-M Fort Huachuca, Ariz.	1
Commanding Officer, USA Electronics Research and Development Laboratories ATTN: SELRA/ADT Fort Monmouth, N. J.	1
Director, USA Development and Proof Services ATTN: Automotive Division Aberdeen Proving Ground, Md.	1
Commanding Officer, Aberdeen Proving Ground ATTN: Tech Library, Bldg. 313 Aberdeen Proving Ground, Md.	2
U. S. Army Materiel Command, Research and Development Division ATTN: Mr. Richard C. Kerr, Bldg. T-7, Room 2051 Washington, D. C.	1
Asst. Chief of Staff for Force Development Hqs, Department of the Army, ATTN: FOR MR RE Washington, D. C.	1

Address	No. of Copies
Chief of Engineers, ATTN: ENGTE-E Department of the Army Washington, D. C.	1
War Plans Division, Engineer Strategic Studies Group Office, Chief of Engineers, U. S. Army Erskine Hall, Army Map Service Washington, D. C.	1
Chief of Engineers, ATTN: ENGAS-I Department of the Army Washington, D. C.	2
CCE (ENGTE) (for Engineer Standardization Program)	4
Commander, U. S. Army Forces Southern Command ATTN: Engineer Fort Amador, Canal Zone	1
Commander, U. S. Combat Development Command ENGINEER AGENCY ATTN: CAGEN-SC Fort Belvoir, Va.	1
Chief of Engineers, ATTN: ENGMC-ER Department of the Army Washington, D. C.	2
The Librarian, U. S. Army Engineer School Library Thayer Hall (Bldg. 270) Fort Belvoir, Va.	2
Hqs, U. S. Continental Army Command Engineer Division, DCSLOG, ATTN: ATLOG-E-MB Fort Monroe, Va.	2
Commanding General, XVIII Airborne Corps ATTN: Corps Engineer Fort Bragg, N. C.	2
Commanding Officer 326th Engineer Battalion Fort Campbell, Ky.	1
Hqs, U. S. Continental Army Command ATTN: ATUTR-AVN Fort Monroe, Va.	1

Address	No. of Copies
United States Army Attaché, American Embassy U. S. Navy 100, Box 36 Fleet Post Office New York, N. Y.	2
Geography Branch, Office of Naval Research Department of the Navy Washington, D. C.	1
Commanding Officer, PHIBCB Two U. S. Naval Amphibious Base Little Creek, Norfolk, Va.	1
Commanding Officer, PHIBCB One U. S. Naval Amphibious Base Coronado, San Diego, Calif.	1
Commanding Officer and Director Naval Civil Engineering Laboratory Port Hueneme, Calif.	1
Director, Naval Warfare Research Center Stanford Research Institute Menlo Park, Calif.	1
Chief, Bureau of Yards and Docks ATTN: Code 42, Department of the Navy Washington, D. C.	2
Commanding Officer, U. S. Naval Photographic Interpretation Center 4301 Suitland Road Washington, D. C.	1
Coastal Studies Institute Louisiana State University Baton Rouge, La.	1
Commander, 3800th AB Wing, AU ATTN: BDCE-ED, Bldg. 78 Maxwell AFB, Ala.	1
Headquarters, USAF (AFRSTC) Astronautics Division DCS/Research and Development Washington, D. C.	1

Address	No. of Copies
Commander, U. S. Strike Command ATTN: J4-E McDill AFB, Fla.	1
Commander, Air Proving Ground Command ATTN: PGABAP-1 Eglin AFB, Fla.	1
Headquarters, Tactical Air Command ATTN: DEDSA Langley AFB, Va.	2
Headquarters, USAF Base Structures Branch, Directorate of Civil Engineering ATTN: AFOCE-GC Washington, D. C.	1
Commander, Hqs, Military Air Transport Service ATTN: MAMCE/FS Scott AFB, Ill.	1
Commander SEG (SEHB) Wright-Patterson AFB, Ohio	1
Headquarters, U. S. Air Force Director of Civil Engineering (AFOCE-KA) Washington, D. C.	2
Library, Division of Public Documents U. S. Government Printing Office Washington, D. C.	1
National Tillage Machinery Laboratory U. S. Department of Agriculture, Box 792 Auburn, Ala.	1
Caterpillar Tractor Company ATTN: Research Library Peoria, Ill.	1
Defense Research Laboratories General Motors Corporation, Box T ATTN: Mr. J. P. Finelli Santa Barbara, Calif.	1

Address	No. of Copies
Engineering Societies Library 345 E. 47th Street New York, N. Y.	1
Commanding General, U. S. Army Tranportation Combat Development Group ATTN: Mr. Earl S. Brown Fort Eustis, Va.	1
Clark Equipment Company Construction Machinery Division, Pipestone Plant Benton Harbor, Mich.	1
Highway Research Board 2101 Constitution Avenue Washington, D. C.	1
Research Analysis Corporation ATTN: Library, 6935 Arlington Road Bethesda, Md.	1
Mr. A. C. Orvedal, Chief, World Soil Geography Unit Soil Conservation Service Room 233A, Federal Center Bldg. Hyattsville, Md.	1
Office of the Chief of Transportation ATTN: TCENG-TE Department of the Army Washington, D. C.	1
Chief, Research and Development ATTN: Chief, Combat Materiel Division Department of the Army Washington, D. C.	1
Chief of Transportation ATTN: Mr. Ch. H. Perry, Deputy Chief of Trans Engrng Div Department of the Army Washington, D. C.	1
Commandant, Command and General Staff College ATTN: Archives Fort Leavenworth, Kans.	1

Address	No. of Copies
Library of Congress Documents Expediting Project Washington, D. C.	3
Chief of Research and Development ATTN: CRD/M, Department of the Army Washington, D. C.	1
New York University, School of Engineering and Science Research Division, University Heights New York, N. Y.	1
Martin Company, ATTN: W. A. Headley, Jr. Research Division, Mail No. MP-383 Orlando, Fla.	1
Commanding Officer, U. S. Army Map Service, Far East ATTN: Area Analysis Division APO San Francisco, Calif.	1
Ohio University Engineering Experiment Station ATTN: Mr. Seth Bonder 159 West 19th Avenue Columbus, Ohio	1
Director, Pacific Southwest Forest and Range Experiment Station, ATTN: Henry W. Anderson P. O. Box 245 Berkeley, Calif.	1
Davidson Laboratory, Stevens Institute of Technology ATTN: Dr. I. R. Ehrlich 711 Hudson Street Hoboken, N. J.	1
Chief, Combat Service Support Division Marine Corps Landing Force Development Center, Marine Corps Schools Quantico, Va.	1
Professor L. C. Stuart University of Michigan Ann Arbor, Mich.	1
Dr. M. G. Bekker GM Defense Research Laboratories General Motors Corporation, Box T Santa Barbara, Calif.	1

Address	No. of Copies
University of Arkansas, College of Engineering ATTN: Mr. Henry H. Hicks, Jr. Fayetteville, Ark.	1
Commanding Officer, U. S. Army General Equipment Test Activity Fort Lee, Va.	1
Office of the AC of S, G2 ATTN: Engineer Intelligence, Hqs Fourth U. S. Army Fort Sam Houston, Tex.	1
Senior Engineer Instructor Office of Military Instruction, United States Corps of Cadets West Point, N. Y.	1
U. S. Geological Survey Chief, Source Material Unit, Branch of Military Geology Washington, D. C.	2
Heavy Construction Section, Department of Engineering Pavements and Materials Group USA Engr School, ATTN: Raymond Hansen Fort Belvoir, Va.	1
Systems Engineering Group, Deputy for Systems Engineering Directorate of Technical Publications and Specifications (SEPRR) Wright-Patterson AFB, Ohio	1
Office of Naval Research, Navy Department ATTN: Mr. Irv. Schiff (Code 493) Washington, D. C.	1
Dr. Clark N. Crain, Director Project DUTY Department of Geography, University of Denver Denver, Colo.	1
Chief, Crops Division U. S. Army Biological Laboratories Ft. Detrick, Md.	1
Jansky and Bailey Division, Atlantic Research Corporation ATTN: Mr. Lester Sturgill Shirley Highway and Edsall Road Alexandria, Va.	1

Address	No. of Copies
Chief, Crops Protection Branch Crops Research Division, Agricultural Research Service Beltsville, Md.	1
Stanford Research Institute ATTN: Mr. Gordon S. Wiley Menlo Park, Calif.	1
Wilson, Nuttall, Raimond Engineers, Inc. ATTN: Dr. Holdridge Chestertown, Md.	1
Wilson, Nuttall, Raimond Engineers, Inc. ATTN: Library Chestertown, Md.	1
Chief, Research and Development Defense Intelligence Agency, ATTN: Special Warfare Office Washington, D. C.	1
Battelle Memorial Institute, ATTN: RACIC 505 King Avenue Columbus, Ohio	1
Commanding Officer, U. S. Army General Equipment Test Activity Fort Lee, Va.	1
Air Force Weapons Laboratory ATTN: Civil Engineering Branch Kirtland AFB, N. Mex.	1
Mr. M. J. McKeown, Supervisor Ordnance Engineering Library, FMC Corporation 1125 Coleman Avenue, Box 367 San Jose, Calif.	1
Commanding Officer, Tropic Test Center P. O. Drawer 942 Fort Clayton, Canal Zone	1
Commanding Officer, U. S. Army Arctic Test Center APO Seattle 98733	1

Address	No. of Copies
Defense Documentation Center, ATTN: Mr. Myer Kahn Cameron Station Alexandria, Va.	20
Terrestrial Sciences Lab (CRJT) Air Force Cambridge Res Lab, L. G. Hanscom Field Bedford, Mass.	1
Foreign Exchange Agreements	
Library National Research Council Ottawa 2, Canada (ENG-17)	1
Dr. William Lucas Archer, Scientific Research Officer Canadian Army Oper Res Estab, Canadian Army Headquarters Ottawa, Canada (ENG-239)	1
Mr. David Cardwell, Asst. Dir., Basic Res. Fighting Vehicles R&D Establishment Chobham Lane, Chertsey Surrey, England (ENG-238)	1
Mr. A. O. Barrie, Ministry of Supply, Mil Engr Experi Estab Barrack Road, Christchurch Hampshire, England (ENG-240)	1
To be forwarded thru Senior Representative, U. S. Army Standardization Group, UK, Keysign House, 429 Oxford Street London, W.1, England	
Mr. F. L. Uffleman, Fighting Vehicles R&D Estab Chobham Lane, Chertsey Surrey, England	1
Prof. P. H. T. Beckett Oxford University, England	1
To be forwarded thru Senior Representative, U. S. Army Standardization Group, Canadian Army Headquarters, Ottawa Ontario, Canada	
Lt. Col. A. L. Maclean Canadian Headquarters Ottawa, Canada	1

Address	No. of Copies
Directorate of Weapons and Engineering Research Canadian Forces Headquarters Ottawa 4, Ontario, Canada	1
Dr. E. G. Leger Canadian Armament R&D Estab Quebec, Canada	1
Mr. T. A. Harwood Defence Research Board Ottawa, Canada	1
Consultants	
Dr. A. A. Warlam	1
Mr. Robert Horonjeff	1
Prof W. Buchele	1
Prof. R. E. Fadum	1
Dr. Gerald Pickett	1
Dr. M. J. Hvorslev	1

Unclassified

Security Classification

DOCUMENT CONTROL DATA - R&D

(Security classification of title, body of abstract and indexing annotation must be entered when the overall report is classified)

1. ORIGINATING ACTIVITY *(Corporate author)*

U. S. Army Engineer Waterways Experiment Station
P. O. Box 631
Vicksburg, Miss.

2a. REPORT SECURITY CLASSIFICATION

Unclassified

2b GROUP

3. REPORT TITLE

STRESSES UNDER MOVING VEHICLES; DISTRIBUTION OF STRESSES BENEATH A TOWED PNEUMATIC TIRE IN AIR-DRY SAND

4. DESCRIPTIVE NOTES *(Type of report and inclusive dates)*

Report 5 of a series

5. AUTHOR(S) *(Last name, first name, initial)*

Green, Andrew J., Jr.

Murphy, Newell R., Jr.

6. REPORT DATE	7a. TOTAL NO. OF PAGES	7b. NO. OF REFS
July 1965	78	5

8a. CONTRACT OR GRANT NO.

b. PROJECT NO. 1-V-0-21701-A-046

c. Task 03

d.

9a. ORIGINATOR'S REPORT NUMBER(S)

Technical Report No. 3-545

Report 5

9b. OTHER REPORT NO(S) *(Any other numbers that may be assigned this report)*

10. AVAILABILITY/LIMITATION NOTICES

Qualified requesters may obtain copies of this report from DDC.

11. SUPPLEMENTARY NOTES

12. SPONSORING MILITARY ACTIVITY

U. S. Army Materiel Command

13. ABSTRACT

Measurements of the magnitude and distribution of normal stresses at the tire-soil interface of an 11.00-20, 12-PR smooth pneumatic tire towed on air-dry mortar sand are presented. Deflection gages inside the tire measured its deflection, and pressure cells embedded in the surface of the tire measured the stresses at the tire-soil interface. Also, pressure cells installed at several depths within the soil mass beneath the center of the tire path measured stresses induced in the soil mass. Results indicate that the distribution of stresses at the tire-soil interface is related to the shape of the deflected tire and thereby to tire load, inflation pressure, and soil strength. Peak stress in the soil mass occurred well ahead of the axle of the test wheel, with the total load on the wheel having the greatest influence on its magnitude. The average stress waves for a tire-soil system such as used in this study can be expressed mathematically in terms of a Fourier series. Application of the Fourier series in stress wave analysis is discussed in Appendix A.

DD FORM 1 JAN 64 1473

Unclassified

Security Classification

14. KEY WORDS	LINK A		LINK B		LINK C	
	ROLE	WT	ROLE	WT	ROLE	WT
Sand Soils Tires Trafficability						

INSTRUCTIONS

1. ORIGINATING ACTIVITY: Enter the name and address of the contractor, subcontractor, grantee, Department of Defense activity or other organization *(corporate author)* issuing the report.

2*a*. REPORT SECURITY CLASSIFICATION: Enter the overall security classification of the report. Indicate whether "Restricted Data" is included. Marking is to be in accordance with appropriate security regulations.

2*b*. GROUP: Automatic downgrading is specified in DoD Directive 5200.10 and Armed Forces Industrial Manual. Enter the group number. Also, when applicable, show that optional markings have been used for Group 3 and Group 4 as authorized.

3. REPORT TITLE: Enter the complete report title in all capital letters. Titles in all cases should be unclassified. If a meaningful title cannot be selected without classification, show title classification in all capitals in parenthesis immediately following the title.

4. DESCRIPTIVE NOTES: If appropriate, enter the type of report, e.g., interim, progress, summary, annual, or final. Give the inclusive dates when a specific reporting period is covered.

5. AUTHOR(S): Enter the name(s) of author(s) as shown on or in the report. Enter last name, first name, middle initial. If military, show rank and branch of service. The name of the principal author is an absolute minimum requirement.

6. REPORT DATE: Enter the date of the report as day, month, year; or month, year. If more than one date appears on the report, use date of publication.

7*a*. TOTAL NUMBER OF PAGES: The total page count should follow normal pagination procedures, i.e., enter the number of pages containing information.

7*b*. NUMBER OF REFERENCES: Enter the total number of references cited in the report.

8*a*. CONTRACT OR GRANT NUMBER: If appropriate, enter the applicable number of the contract or grant under which the report was written.

8*b*, 8*c*, & 8*d*. PROJECT NUMBER: Enter the appropriate military department identification, such as project number, subproject number, system numbers, task number, etc.

9*a*. ORIGINATOR'S REPORT NUMBER(S): Enter the official report number by which the document will be identified and controlled by the originating activity. This number must be unique to this report.

9*b*. OTHER REPORT NUMBER(S): If the report has been assigned any other report numbers *(either by the originator or by the sponsor)*, also enter this number(s).

10. AVAILABILITY/LIMITATION NOTICES: Enter any limitations on further dissemination of the report, other than those imposed by security classification, using standard statements such as:

(1) "Qualified requesters may obtain copies of this report from DDC."

(2) "Foreign announcement and dissemination of this report by DDC is not authorized."

(3) "U. S. Government agencies may obtain copies of this report directly from DDC. Other qualified DDC users shall request through _____."

(4) "U. S. military agencies may obtain copies of this report directly from DDC. Other qualified users shall request through _____."

(5) "All distribution of this report is controlled. Qualified DDC users shall request through _____."

If the report has been furnished to the Office of Technical Services, Department of Commerce, for sale to the public, indicate this fact and enter the price, if known.

11. SUPPLEMENTARY NOTES: Use for additional explanatory notes.

12. SPONSORING MILITARY ACTIVITY: Enter the name of the departmental project office or laboratory sponsoring *(paying for)* the research and development. Include address.

13. ABSTRACT: Enter an abstract giving a brief and factual summary of the document indicative of the report, even though it may also appear elsewhere in the body of the technical report. If additional space is required, a continuation sheet shall be attached.

It is highly desirable that the abstract of classified reports be unclassified. Each paragraph of the abstract shall end with an indication of the military security classification of the information in the paragraph, represented as *(TS)*, *(S)*, *(C)*, or *(U)*.

There is no limitation on the length of the abstract. However, the suggested length is from 150 to 225 words.

14. KEY WORDS: Key words are technically meaningful terms or short phrases that characterize a report and may be used as index entries for cataloging the report. Key words must be selected so that no security classification is required. Identifiers, such as equipment model designation, trade name, military project code name, geographic location, may be used as key words but will be followed by an indication of technical context. The assignment of links, rules, and weights is optional.